HIGH GAS BARRIER POLYELECTROLYTE COMPLEX THIN FILMS

A Dissertation

by

HSU-CHENG CHIANG

Submitted to the Graduate and Professional School of
Texas A&M University
in partial fulfillment of the requirements for the degree of

DOCTOR OF PHILOSOPHY

Chair of Committee,	Jaime Grunlan
Committee Members,	Emily Pentzer
	Xin Yan
	Yossef Elabd
Head of Department,	Simon North

August 2022

Major Subject: Chemistry

ABSTRACT

Polymeric thin films with high oxygen barrier are important for extending the shelf life of food and protecting electronic devices. Polyelectrolyte complex (PEC) thin films impart super gas barrier, good adhesion, and low-cost processing. However, current PEC films fabricated via layer-by-layer assembly require numerous processing steps, which limits commercial applications. To deposit films with fewer deposition steps, PEC suspensions can be applied in a single step. This dissertation is focused on understanding, improving, and extending the utility of PEC-based gas barrier thin films.

A PEC coacervate composed of branched polyethyleneimine (PEI), poly(acrylic acid) (PAA), and kaolinite clay (KAO) was applied using bar-coating. The shear-induced alignment of a nano-brick wall structure lead to coatings that are less sensitive to humidity. PECs made with various molar ratios of PEI and PAA were prepared as one-pot coating solutions, which can be deposited via a simple dip-coating process and cured with a citric acid buffer solution. As-prepared conformal thin films impart excellent gas barrier, high modulus, and high moisture resistance. The strong complexation from ionic crosslinking creates an unusually dense thin film that is promising for various packaging applications. An edible PEC film consisting of chitosan (CH) and pectin (PT) was developed and deposited on bananas and apple slices. This edible coating slows the aging and browning of these fruits. The ability to extend the shelf life of fresh fruit and vegetables could reduce food waste. These direct-deposited PEC thin films have great potential for various gas barrier applications.

DEDICATION

This dissertation is dedicated to my dearest parents for their constant love and support. I am truly thankful for having them in my life.

ACKNOWLEDGEMENTS

I would like to express my sincerest appreciation to my research adviser, Dr. Jaime Grunlan, for his guidance and support during my time here at Texas A&M. I am grateful for his valuable advice throughout my PhD, which also helps me for my future career. I would also like to thank my committee members, Dr. Emily Pantzer, Dr. Xin Yan, and Dr. Yossef Elabd for their expertise throughout the course of my research.

I would also like to appreciate my colleagues in Polymer Nanocomposite Laboratory, including Dr. Shuang Qin, Dr. Simone Lazar, Dr. Dan Stevens, Dr. Thomas Kolibaba, Dr. Carolyn Long, Bethany Palen, Natalie Vest, Ethan Iverson, Danixa Rodriguez Melendez, and Dallin Smith. Their friendship and support bring me the best memory in PhD. I also thank my undergraduate assistants, Bailey Eberle, Drew Carlton, and Kendra Schmieg. I could not finish these studies without their contributions.

A special shout out goes out to my Taiwanese cohort, Katherine Wang, Ching Pang, and Tony Lai for making PhD program an enjoyable experience.

Thanks also go to my mentors at National Taiwan University. I would not have made it this far without the help and support from Dr. Yit-Tsong Chen, Dr. Chiao-Chen Chen, Dr. Subhasree Banerjee, and Dr. Chi-Ang Tseng.

Lastly, I would like to thank my parents for their love and sacrifices. I love you.

CONTRIBUTORS AND FUNDING SOURCES

Contributors:

This work was supervised by Professor Jaime Grunlan, and the rest of the dissertation committee including Professor Emily Pantzer and Professor Xin Yan of the Department of Chemistry, and Professor Yossef Elabd of the Department of Chemical Engineering.

All work conducted for this dissertation was completed by Hsu-Cheng Chiang with the help from Grunlan's research group.

Funding Sources:

All work presented herein was infrastructurally and financially supported by the Texas A&M Engineering Experiment Station (TEES).

NOMENCLATURE

AFM	Atomic Force Microscope
CH	Chitosan
CVD	Chemical Vapor Deposition
KAO	Kaolinite
LbL	Layer-by-layer Assembly
MMT	Montmorillonite
OTR	Oxygen Transmission Rate
PAA	Poly(acrylic acid)
PDDA	Poly(diallydimethylammonium chloride)
PEI	Polyethyleneimine
PEC	Polyelectrolyte Complex
PEO	Poly(ethylene oxide)
PET	Poly(ethylene terephthalate)
PT	Pectin
PVD	Physical Vapor Deposition
QCM	Quartz Crystal Microbalance
SEM	Scanning Electron Microscopy
SiOx	Silicon Oxide
TEM	Transmission Electron Microscopy
UV-vis	Ultraviolet–Visible

TABLE OF CONTENTS

Page

LIST OF FIGURES

Page

LIST OF TABLES

Page

CHAPTER I

INTRODUCTION

1.1 Background

High oxygen barrier thin films for packaging are of great interest to improve the shelf life of pharmaceuticals, reduce food waste, and protect flexible electronics.[1–3] Inorganic gas barrier layers, such as metal and metal oxide thin films, have serious drawbacks.[4,5] These inorganic barriers have low oxygen permeability and wide acceptance, but the opaqueness and difficult recycling of metalized plastic films, and the rigidity, poor adhesion, and costly vacuum-based processing of metal oxide films (e.g. SiO_x and Al_xO_y), severely limit their utility.[6,7] To overcome these limitations, polymer coatings prepared via layer-by-layer (LbL) assembly have been developed to exhibit optical transparency, microwave compatibility, and better flexibility than their inorganic counterparts.[8] Films assembled with polymers and clay platelets exhibit remarkable gas barrier performance due to the tortuous pathway that forces gas molecules to move around aligned clay platelets during permeation. These sub-micron, clay-based films also exhibit very high transparency, which is unique compared to other clay-based composites.[9–11] These multilayer nanocoatings are of great interest due to their low cost raw materials and environmentally benign processing.

While LbL assembly provides many advantages, the numerous processing steps remains a major challenge for commercial applications.[12,13] It would be a significant achievement to deposit a similar structure in a single processing step. In order to deposit films with fewer deposition steps, aqueous solutions of polyelectrolyte complexes (PEC)

have recently been exploited to fabricate oxygen barrier thin films in a single step.[14,15] Mixing polyelectrolytes of opposite charge can result in an insoluble complex, metastable coacervate, or soluble solution.[16] This entropy-driven complexation is governed by the intrinsic (polycation−polyanion) and extrinsic (polyelectrolyte−counterion) pairs, which can be tuned by altering pH and salt concentration, respectively.[17] When the electrostatic interactions between the polyelectrolytes are limited, a liquid-liquid phase-separated mixture is formed and consists of a polymer-rich phase (coacervate) and a polymer poor solution phase. The PEC coacervate has viscous liquid-like properties that are suitable for quick thin-film deposition, but all-polymer (i.e. polymer-only) coatings are sensitive to moisture.[18] In an effort to reduce the moisture sensitivity and further improve the gas barrier, clay nanoplatelets can be incorporated in these polymeric coatings.[19,20]

Due to the growing interest in environmental friendliness, bio-based materials have received more attention as an alternative to synthetic polyelectrolytes. Natural materials including polysaccharides, proteins, and lipids have been increasingly used in post-harvest preservation of fruits and vegetables.[21–23] Non-toxic, edible ingredients for high gas barriers coating not only makes this technology promising for improving shelf life. Its biodegradability also contributes to the reduction of environmental effluence by reducing use of normal plastic food packaging. The work described in this dissertation demonstrates promising approaches to fabricate high gas barrier films. The studies outlined here utilize water-based, low-cost components and ambient conditions for deposition, which is essential for industrial applications.

1.2 Dissertation Outline

Chapter II provides an overview of gas barrier thin films and polyelectrolyte complexes. The first part introduces commonly used oxygen barrier thin films, including inorganic gas barrier (metal and oxide coatings) and organic gas barrier (polymer composites and LbL assembly of polyelectrolytes). The second part of the chapter reviews polyelectrolytes complexes.

Chapter III describes a new strategy of using a PEC/clay coacervate to create a high gas barrier thin film with moisture resistance. By incorporating kaolinite (KAO) clay into branched polyethyleneimine (PEI) and poly(acrylic acid) (PAA), the PEC/clay coacervate can be deposited as a high gas barrier film in a single step through shear-induced clay alignment, providing PET with more than three orders of magnitude reduction in oxygen transmission rate (OTR), while also achieving high transparency and moisture resistance.

Chapter IV illustrates a unique water-based coating deposited as a one-pot polyelectrolyte complex consisting of various molar ratios PEI and PAA. The strong complexation after buffer-curing creates a dense film that imparts excellent gas barrier, high modulus, and surprising moisture resistance. A sub-micron PEI/PAA film reduces the oxygen transmission rate of 179 μm thick polyester by more than three orders of magnitude under both dry and humid conditions. This is one of the best polymer-based oxygen barriers ever reported, with undetectable OTR at 90% RH, without using chemical crosslinking or fillers.

Chapter V demonstrates an edible PEC film consisting of chitosan (CH) and pectin (PT), which can be directly deposited on bananas and apple slices. This edible coating slows the aging and browning of these fruits. The ability to extend the shelf life of fresh fruit and vegetables could reduce significant food waste.

Chapter VI provides conclusions and outlines two potential future studies. This dissertation demonstrates the effectiveness of PEC thin films as gas barriers coatings. Going forward, a Diels-Alder-based PEC coating is proposed to impart self-healing and improve the moisture barrier of these water-based coatings. Diels–Alder reaction can make a reversible crosslinked structure, which has better durability due to its self-healing behavior. Another proposed study involves an edible crosslinking chemistry. Edible PEC coatings made from chitosan and gelatin can be crosslinked by riboflavin to improve the moisture resistance. These studies illustrate simple strategies to develop industrially feasible gas barrier coatings that encompass processability, environmental friendliness, and durability.

CHAPTER II

LITERATURE REVIEW

2.1 Gas Barrier Thin Films

Gas barrier films are important to extend the life of food, pharmaceutical, and electronics due to the low oxygen permeability.[8,24,25] **Figure II-1** illustrates the barrier properties required for various packaging applications. Metalized plastic is the most commonly used packaging material due to its high barrier and low cost. Metalized plastic also lacks transparency and is difficult to recycle.[26] Inorganic oxide barrier coatings, such as SiO_x or Al_xO_y, impart good barrier and optical clarity, but poor adhesion and inherent pinholes limit their utility.[27,28] Polymers are widely used as packaging materials over the past few decades due to low cost, ease of production, and tunable properties. More than 40% of synthetic polymers, including polyethylene (PE), polypropylene (PP), polystyrene (PS), and polyethylene terephthalate (PET) are produced as packaging materials in the form of bottles, boxes, and films.[29] The intrinsically high gas permeability of these polymer materials (as shown in **Figure II-2**) limits their ability to protect sensitive food, medicine, and electronic displays. Biodegradable gas barrier materials are also being studied to reduce plastic waste and carbon emissions.[24] Besides the conventional inorganic gas barrier coating, polymer composite coatings impart high gas barrier by creating higher tortuosity for gas molecules. Various gas barrier coatings will be discussed here along with their corresponding challenges.

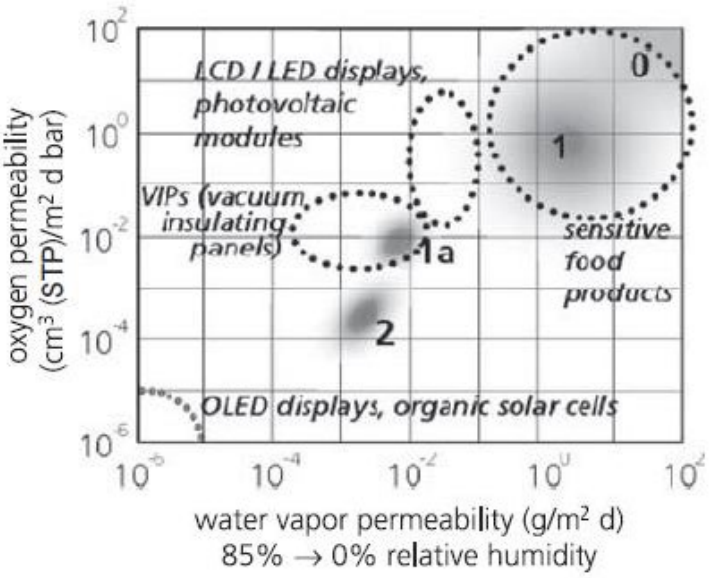

Figure II-1. Barrier properties required for various packaging applications (dotted circles). The numbers represent the performance of packaging materials: (0) polymer substrates alone, (1) inorganic coatings, (2) inorganic/polymeric multilayer system. Reprinted from [reference 30].[30]

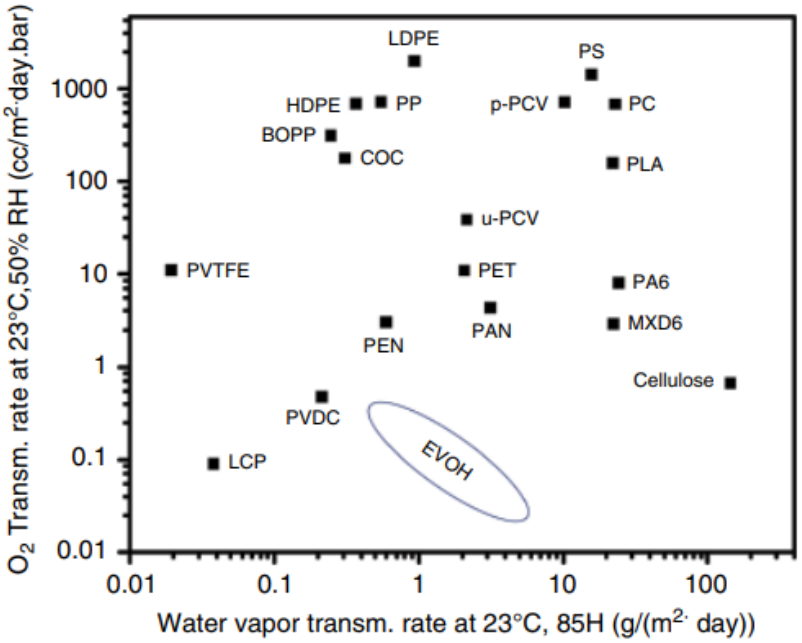

Figure II-2. Oxygen and water transmission rates of commonly used polymers in packaging. Reprinted from [reference 31].[31]

2.1.1 Inorganic Gas Barrier

Inorganic layers are commonly deposited on polymer materials under vacuum to improve the gas barrier, which represent the first gas barrier coatings.[1] More than 15 billion square meters of these inorganic gas barrier coatings are consumed each year.[30] These inorganic coatings reduce the gas permeability up to three orders of magnitude compared to uncoated polymer substrates like PET, PP, etc.[32] **Table II-1** lists oxygen transmission rate (OTR) and water vapor transmission rate (WVTR) of some inorganic thin film coatings. The two most common inorganic barrier coatings, metal thin film coatings and transparent oxide coatings, will be discussed in this section.

Table II-1. Barrier properties of inorganic thin film coatings. Reprinted from [reference 2].[2]

Normalized to 1 mil thickness	OTR (cm^3(STP)/m^2 per day per atm)	WVTR (g/m^2 per day) at 90–100% RH	Deposition method
PET/SiO_x a	2.0	1.1	Evaporation
PET/SiO_x c	0.08	0.5	PECVD
PET/AlO_x	1.5	5.0	Evaporation
PET/AlO_xN_y	2.8	4.3	Sputtering
PET/DLC	2	1.5	PECVD
PET/ITO	1.56	0.2	Sputtering
PET/Al	0.31–1.55	0.31–1.55	Evaporation
Nylon/Al	0.8	3.1	Evaporation
PET/7 mm Al foil	0.001	—	Lamination
PET	79	10.7	—

2.1.1.1 Metal Thin Film Coating

Metal thin film deposition under vacuum has been widely used as a gas barrier since the 1970s.[33] The coating is normally deposited through physical vapor deposition (PVD) at a deposition rates of several nm per second. Metal elements or alloy are vaporized in a vacuum environment and then condensed on the polymer substrate.[34] Thermal vaporization and sputter vaporization use heat and high energy electron beams to evaporate the coating materials.[35] Arc vapor deposition and ion plating techniques have also been used for PVD.[36] High vacuum is required to eliminate the collision between gas molecule and coating material. Microscopic defects are often present on the substrate surface due to geometrical shadowing (as shown in **Figure II-3**) or weak adsorption, which leads to pinholes, poor surface coverage.[36,37] These issues are normally alleviated by improving vacuum conditions and reducing thermal and mechanical stress.[38]

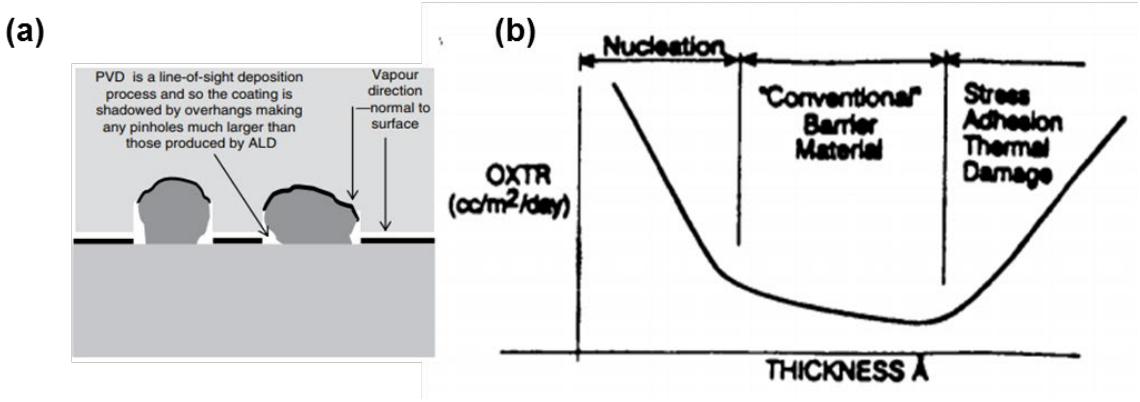

Figure II-3. (a) Schematic of the shadowing effect in the PVD process.[31] **(b)** Illustration of oxygen transmission rate as a function of thickness.[39] Adapted with permission from [reference 31 and 39].[31,39]

Among the wide range of metals and alloys, aluminum is the most used material to deposit flexible barrier coatings with low oxygen transmission rate and water vapor

transmission rate.[38] Although metal thin films exhibit high oxygen and moisture barrier at low cost, they are not transparent or microwavable.[26] Recyclability is another concern that negatively impacts the environment. Although a cryogenic process has been evaluated to liberate metal from the polymer substrate, the high cost of recycling remains a major challenge.[40]

Table II-2. OTR and WVTR values of metal thin film coating on commonly used polymer substrates. Reprinted from [reference 2].[2]

Film	Thickness (μm)	OTR ($cm^3\ m^{-2}\ d^{-1}$)	WVTR ($g\ m^{-2}\ d^{-1}$)
PET film	25	31–93	16–20
PET film, metallized	25	0.16–1.7	<1.0
OPP film	25	1550–2500	3.9–6.2
OPP film, metallized	25	19–160	<0.6

2.1.1.2 Transparent Oxide Coating

A small fraction of inorganic gas barrier coatings are made from transparent oxides such as silicon oxide (SiO_x) or aluminum oxide (Al_xO_y). SiO_x or Al_xO_y can be deposited through PVD or chemical vapor deposition (CVD).[41] **Figure II-4** shows a roll-to-roll CVD coater using organosilane and oxygen to deposit an SiO_x coating.[27]

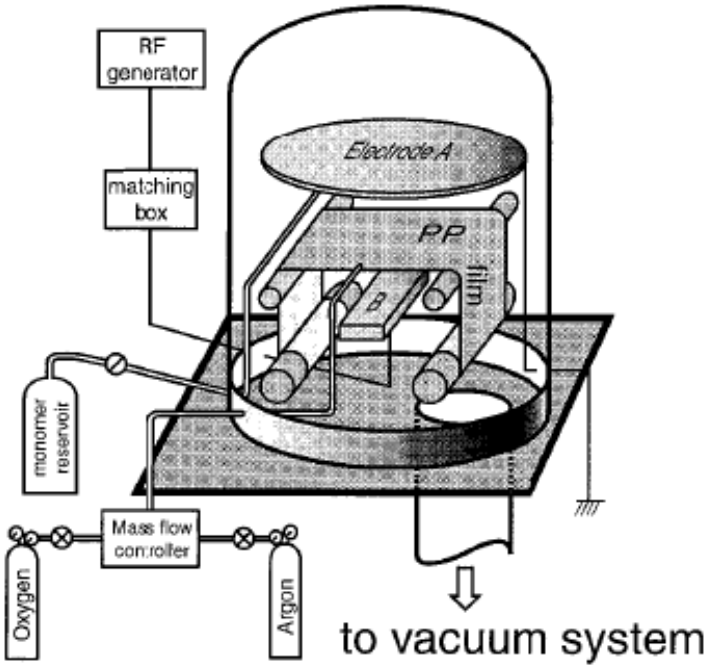

Figure II-4. Schematic of a roll-to-roll CVD deposition apparatus. Reprinted from [reference 27].[27]

Similar to metalized plastics, transparent oxide coatings impart high gas barrier if no significant defects exist.[1,32,42] A 100 nm thick SiO_x coating improves the oxygen barrier of PET by more than two orders of magnitude.[43] Microscopic defects are also observed due to the aforementioned shadowing effect. There are also grain boundaries of SiOx from this nonequilibrium thermodynamic coating process. Transparent oxide coatings also suffer from extensive cracking upon stretching due to brittleness. **Figure II-5** shows the image of poorly coated SiOx on PP.[44] These defects can significantly deteriorate barrier. Although transparent oxide coatings have been commercially available for decades, their applications are limited due to the inherent brittleness of silicon/aluminum oxide and poor adhesion to polymer substrates.

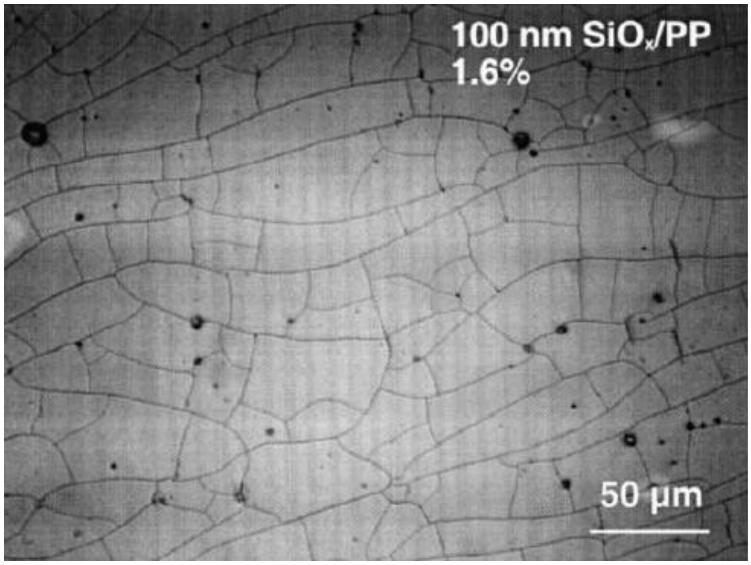

Figure II-5. Surface image of 100 nm SiO_x coated on polypropylene substrate. Reprinted from [reference 44].[44]

2.1.2 Polymeric Gas Barrier

Polyethylene (PE), polypropylene (PP), polystyrene (PS), and polyethylene terephthalate (PET) have been extensively used as packaging materials due to their low cost and good mechanical properties. The solution-diffusion model can describe gas permeability of dense, non-porous polymer films.[45] The air pressure across a polymer film acts a driving force, leading to gas dissolution into the membrane, followed by diffusion and desorption. The gas solubility is thermodynamically controlled by the interaction between gas and polymer matrix.[46] While diffusion is the rate-controlling process, which depends on the mobility of the gas molecule in a polymer matrix. The gas mobility is predominately affected by the free volume in the polymer matrix. The smaller the free volume, the "denser" the polymer film and the better barrier it has.[47] Stiffer polymers with

high crystallinity and side groups that interact with gas molecules (through hydrogen bonding or polar-to-polar interaction) generally exhibit better gas barrier, but still require a gas barrier coating for various packaging applications. Polymer composites have improved barrier, mechanical, electrical, and thermal properties over neat polymers.[48,49]

Polymer composites have been widely studied for various applications including drug delivery,[50,51] antibacterial,[52] and packaging.[53] The first commercial example is a clay/nylon composite used in the automotive industry.[54] Polymer composites can be prepared by blending.[29,55] A variety of inorganic fillers can be incorporated into the polymeric matrix, including TiO_2,[56] Ag,[57] clay,[58] and carbon nanomaterials (carbon nanotubes, graphene).[59] Among different fillers, natural clay platelets are the most used due to their natural abundance and intercalation ability.[60,61] Clay in a polymer matrix has three possible morphologies, including tactoid, intercalated, and exfoliated, as shown in **Figure II-6**.[53] Clay platelets are impermeable to most gases, thus the clay dispersion significantly affects the oxygen barrier.[53,60] Random clay alignment in the polymer matrix has the lowest gas barrier and causes low visible light transmission, which is unfavorable for most applications.[8] With that said, excellent clay dispersion in polymer matrices is important, but challenging due to the incompatibility between clay and polymer. Approaches for better dispersion include surface modification,[62] in-situ polymerization, and melt blending.[63,64] These techniques have been studied to improve composite performance.[53,60,65] Melt blending is compatible with the current compounding devices such as extrusion and injection molding, which makes it feasible for industrial-scale production.[66]

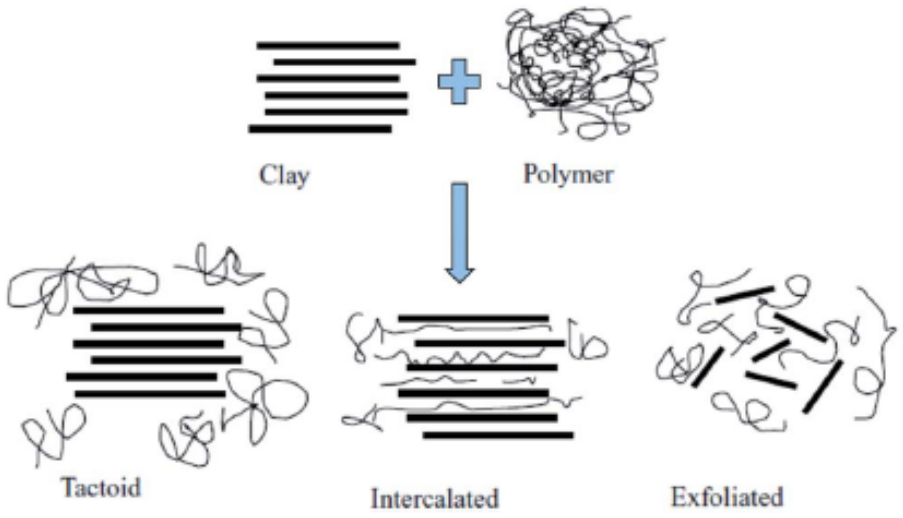

Figure II-6. Schematic of possible polymer/clay composites morphologies. Reprinted from [reference 53].[53]

The addition of nanofillers improves gas barrier of the polymer matrix by creating tortuous diffusion pathways. The polymer composites consist of a permeable polymer matrix and impermeable nanoplatelets. In the tortuous pathway model, the diffusion coefficient D is expressed as:[46]

$$D = \frac{D_0}{\tau}$$

where D_0 is the diffusion coefficient of the polymer matrix and τ is the tortuosity of the composite, which is defined as the ratio of distance that a gas molecule must travel through. **Figure II-7** shows how the tortuous pathway has a major influence on the gas permeability of the composites. When the clay platelets are parallel aligned to the substrate, τ is given as:

$$\tau = 1 + \frac{L}{2W}\phi$$

where ϕ, L and W are volume fraction, length and thickness of the nanoplatelets, respectively. This equation suggests that increasing volume fraction and aspect ratio decreases the diffusion coefficient and thus reduces permeability. Volume fraction is limited by the clay aggregation and misalignment, while aspect ratio is determined by the clay characteristics. It can be concluded that clay dispersion and clay type greatly affect gas barrier. The oxygen barrier of some polymer/clay composites is listed in **Table II-3**.[29]

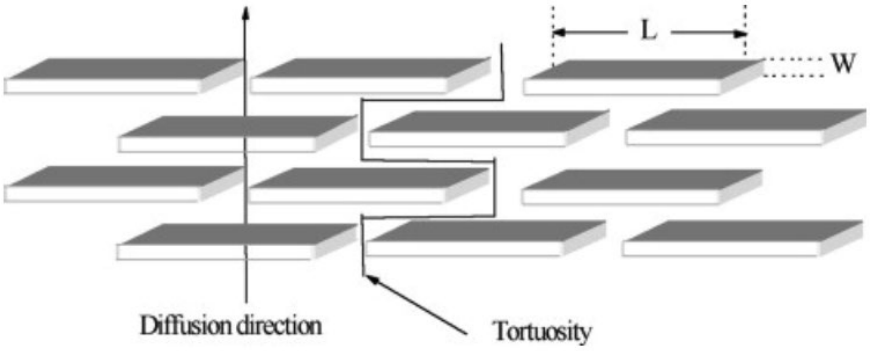

Figure II-7. Schematic of the tortuous pathway in polymer/clay composites. Reprinted from [reference 46].[46]

Table II-3. Oxygen permeability of polymer/clay composites. Reprinted from [reference 29].[29]

Polymer	Types of clay	Filler loading	Processing [a]	Permeant	Permeability ($m^2\ s^{-1}\ Pa^{-1}$)	Reduction
SBR[18]	O-MMT, CF	16 phr	Melt	O_2	2.75×10^{-17}	46%
PLA[120]	O-MMT	7.9 wt%	Melt	O_2	2.85×10^{-18}	24%
				He	6.79×10^{-17}	23%
PLA, PLA/PCL[121]	O-MMT	3 wt%	Melt	O_2	6.39×10^{-19}	26%
PA[122]	MMT	3 wt%	Melt	O_2	3.37×10^{-19}	14%
				CO_2	1.33×10^{-18}	13%
PET[123]	O-MMT	5 wt%	Melt	O_2	1.69×10^{-19}	55%
PET[124]	O-MMT	5 wt%	Melt	O_2	2.74×10^{-19}	69%
PET[125]	O-MMT	1 wt%	Melt	O_2	1.42×10^{-17}	45%
PS[126]	O-MMT	2 wt%	Melt	O_2	N/A	66%
PP[127]	O-MMT	4 vol%	Melt	O_2	4.18×10^{-18}	46%
PP[128]	O-MMT	7.5 wt%	Melt	O_2	2.59×10^{-15}	56%
PP[129]	MMT, O-MMT	5 wt%	Melt	O_2	$\sim 6.00 \times 10^{-18}$	77%

In order to achieve highly ordered and defect free layered structures, layer-by-layer assembly (LbL) is an ideal technique due to its simplicity and versatility.[12] LbL thin films have been widely used for a variety of applications including gas barrier and gas separation coatings.[67,68] Kotov *et. al.* reported the first LbL gas barrier membrane assembled with montmorillonite MMT and poly(diallyldimethylammonium) chloride in 1998.[69] LbL assemblies of polyelectrolyte/clay impart transparency, flexibility, and super gas barrier on various substrates due to a highly ordered multilayer structure.[70–72] **Figure II-8** shows this highly ordered polymer/clay multilayer structure.[73,74] The oxygen permeability of a 80 nm thick (10 bilayers) PEI/MMT multilayer coating is as low as 2.9×10^{-20} cm^3 cm^{-2} s^{-1} Pa^{-1}.[73] This PEI/MMT multilayer coating has been further improved through pH and ionic strength manipulation of the MMT suspension to achieve edge-to-edge clay alignment.[75] Larger clay spacing (**Figure II-8b**) of a PEI/PAA/PEI/MMT quadlayer film creates a longer diffusion path between the clay layers. This 50 nm thick (5 quadlayers) polymer/MMT multilayer film reduces OTR of the PET substrate below the detection limit of commercial instrumentation (< 0.005 cm^3 m^{-2} day^{-1}) with 95% visible light transmission.[74] LbL polymer composite gas barrier coatings eliminate the use of vacuum, while maintaining the desired properties of an inorganic coating.[76,77] **Figure II-9** clearly shows the superiority of these LbL coating relative to other prevalent technologies. As LbL technology and polyelectrolyte complexation progress (will be discussed in **Section 2.2**), commercial polymer gas barrier coatings will likely appear.[8]

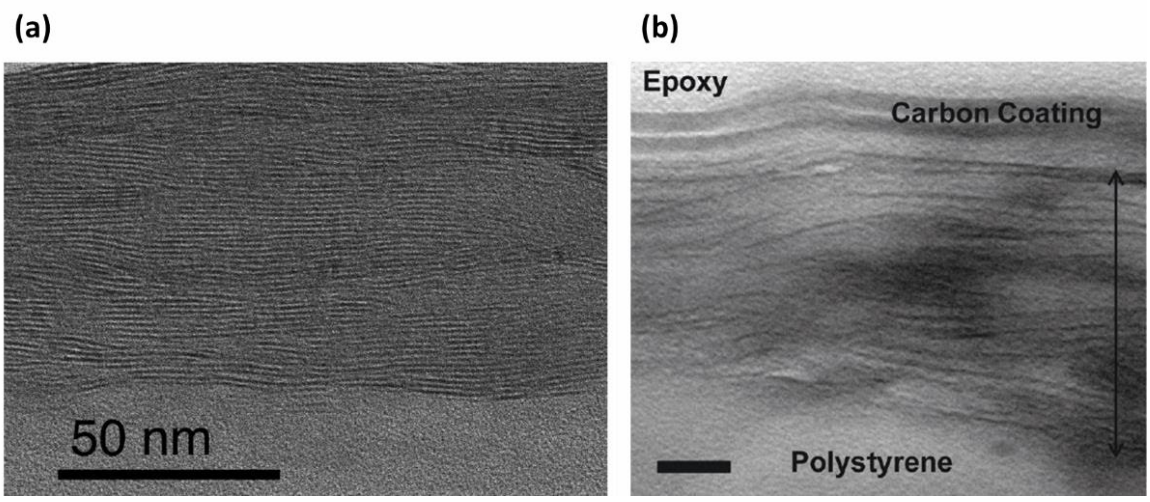

Figure II-8. TEM cross-sectional images of **(a)** 10 bilayers of PEI/MMT[73] and **(b)** 5 quadlayers of PEI/PAA/PEI/MMT. Reprinted from [reference 74].[74]

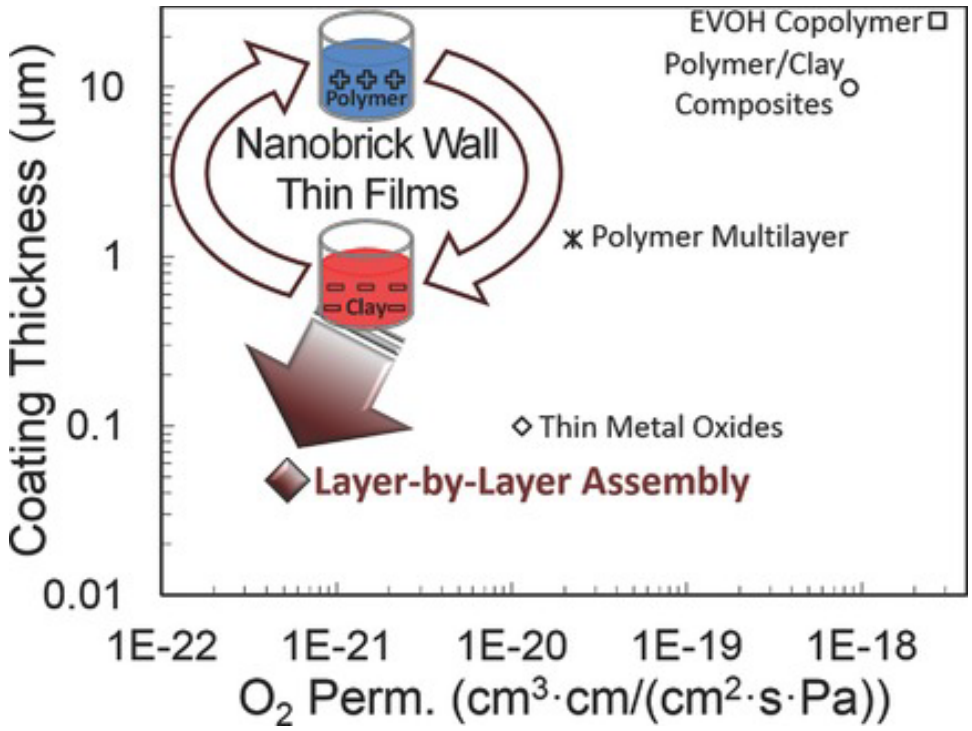

Figure II-9. Gas barrier coating thickness as a function of oxygen permeability. Reprinted from [reference 8].[8]

2.2 Polyelectrolyte Complexes

Polyelectrolytes are macromolecules that exhibit some degree of charge density depending on monomer chemistry. Polyelectrolytes often have excellent solubility in water, making them good candidates for water-based polymer coating systems. Polyelectrolytes are considered strong if they lack charge density dependence on pH, or weak if their charge density chiefly depends on pH in aqueous media. The positively charged polycations are usually amine-based, such as poly(diallydimethylammonium chloride) (PDDA) and polyethylenimine (PEI). Polyanions typically have acid carboxylate, sulphonate, or phosphate moieties (e.g. poly(acrylic acid) (PAA), poly(styrene sulfonate) (PSS), and poly(sodium phosphate) (PSP), respectively).

Polyelectrolyte complexation occurs when two oppositely charged polyelectrolytes are mixed.[78] Polyelectrolyte complexes (PEC) in aqueous media have different forms ranging from insoluble precipitates,[79] liquid-like coacervates,[17,80] to homogenous solutions[15] depending on pH and salt concentration (**Figure II-10**). The formation of PEC, is driven by the entropy change from the expelling of counterions held by charged polyelectrolytes.[81] This entropic gain of the counterions expulsion outweighs the losses of mobility and free volume within the polyelectrolyte chains. There are two different types of ion pairs in this charged polyelectrolyte assembly. Intrinsic ion pairs are polycation−polyanion pairs, and extrinsic ion pairs are polyelectrolyte−counterion pairs. **Figure II-11** shows the new ionic bonds formed between polyelectrolytes. By altering pH and salt concentration, these intrinsic and extrinsic pairs can be compensated, respectively, resulting in different types of PEC. The formation and reaction conditions of these complexes were first explored in 1929.[82,83]

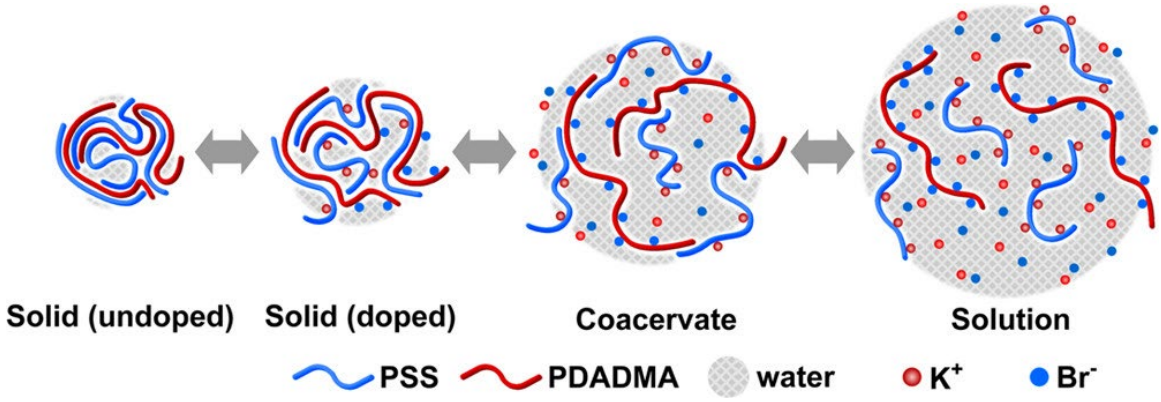

Figure II-10. Schematic of microstructures of PEC solid, coacervate, and solution. Reprinted from [reference 16].[16]

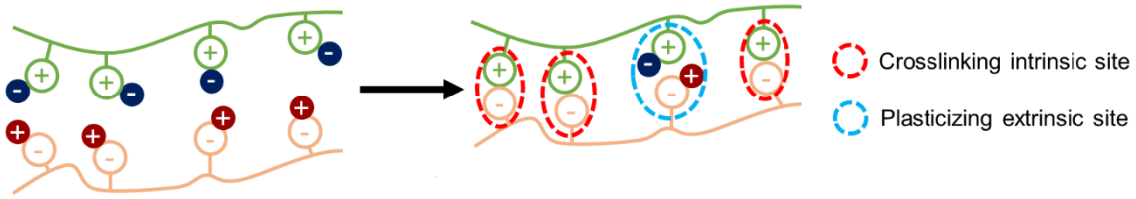

Figure II-11. Schematic of the formation of a polyelectrolyte complex. When extrinsic ion-pairings are no longer plasticized, oppositely charged polyelectrolytes are ionically crosslinked.

The first evaluation of an insoluble PEC was reported in 1949, where the turbidity was measured of different suspensions of polyacrylate and poly-4-vinyl-*n*-*N*-butylpyridonium bromide complexes.[79] The insoluble solid or suspended microparticles form due to strong electrostatic interactions between polycations and polyanions, depending on ionic strength and mixing ratio.[84] When an ideal amount of counterions (e.g. salts) is introduced to a PEC mixture, coulombic interactions will be shielded and the polyelectrolytes will loosely associate with one another. Since the coulombic interactions

are not strong enough to expel small ions and water, a viscous liquid-like substance called a coacervate forms instead of a solid complex.[85] Coacervates can be found between two strong polyelectrolytes such as PDDA and PSS with salt addition.[16,86] It can also be found between strong and weak polyelectrolytes through manipulation of pH and ionic strength. Their viscosity can be tuned with salt content and pH.[87,88] Coacervates have some degree of microscopic phase separation, which will coalesce into a macroscopic phase separation with longer time and elevated temperature.[84] Fu *et al*. found that the association strength of different polyelectrolyte pairs varies based on the concentration of KBr salt used.[89] They suggest that weak polyanions like PAA are better suited for coacervate formation. Strong polyelectrolytes like PSS form strong/glassy complexes that are more resistant to salt-doping. When the association is further compensated, a PEC solution without phase separation can be achieved. The liquid-like coacervate and homogenous PEC solution have significant potential to develop direct deposition as functional PEC thin films due to their ease of processing.

Before direct PEC deposition had been developed, the most well-established method for depositing polyelectrolyte thin films was layer-by-layer assembly. Instead of depositing polyelectrolytes simultaneously, LbL uses a sequential process to assemble thin films by alternate immersions in solutions containing each component. Iler first reported this type of sequential deposition using oppositely charged colloidal particles in 1966.[90] The LbL assembly of oppositely charged polyelectrolytes was first reported by Decher in 1992.[91] These multilayer PEC thin films have been studied and developed over the last 30 years, demonstrating ease of processing, precise tailorablity, and environmental

friendliness.[12] This LbL technique predominantly utilizes electrostatic interactions between charged polyelectrolytes (or a variety of donor/acceptor interactions).[92,93] The sequential process involves the alternate immersion of a charged substrate in polyelectrolyte solutions to sequentially form a PEC.[93–95] The polyelectrolyte adsorbs to the substrate through electrostatic and van der Waal's interactions. The loosely adhered polyelectrolytes are typically rinsed off throughout the process. The substrate is then exposed to oppositely charged polyelectrolytes or nanofillers.

The interface between a growing LbL film and a polyelectrolyte solution progressively builds a PEC on a surface throughout this process. The PEC films behave as heavily crosslinked materials because of the extensive ionic bonds.[96] This LbL process can be achieved by dipping,[94,97,98] spraying,[99–101] or spin coating.[102–104] Versatility is one of the factors that leads to the popularity of LbL assembly as a research field. Besides electrostatic interactions, other complimentary interactions can be used, such as hydrogen bonding.[105–107] Properties of the LbL film, such as thickness and morphology, can be tailored by changing temperature,[108,109] pH,[110–112] ionic strength,[113,114] and buffering capacity.[115,116] Examples of how solution pH and ionic strength influence LbL films is demonstrated in **Figure II-12**. LbL systems can construct bilayer,[117,118] trilayer,[119,120] or quadlayer[121–123] assemblies and can incorporate many chemistries into a polymer composite coating. Due to the flexibility of this technique, a wide array of application are possible: gas barrier,[8,118] flame retardancy,[124,125] anti-reflection,[126,127] anti-corrosion,[128,129] and dielectric.[130]

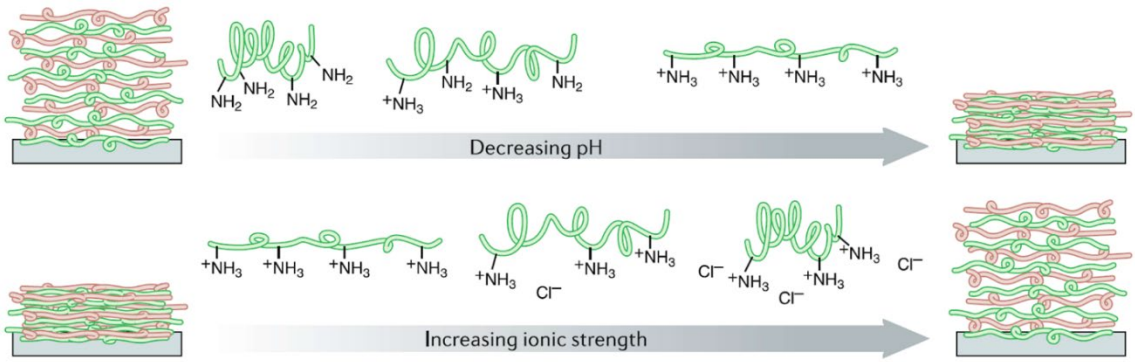

Figure II-12. Illustration of the influence that solution pH and ionic strength have on the morphology and thickness of PEC coating. Reprinted from [reference 125].[125]

Despite the advantages of LbL assembly, the number of processing steps significantly limits commercialization of this technique.[13,93] Efforts have been made to make PEC coatings more commercially viable. Methods for PEC deposition in fewer steps have received some recent attention. One method involves spraying two polyelectrolytes onto a surface simultaneously.[131] As the two solutions come into contact with one another, the PEC forms on the substrate. Film thickness increases linearly as a function of spraying time. Coacervates were also evaluated as a coating solution for depositing a PEC in a single step. Kelly *et al.* spin coated a PDDA/PSS coacervates to create free-standing 15 μm films.[86] Haile *et al*. deposited a PEI/PAA coacervate via Meyer-rod, which produced a high oxygen barrier layer.[14] This as-coated film was cured in citric acid buffer, which reduces free volume of the PEC film through electrostatic interaction. Smith *et al*. deposited a PDDA/PAA thin film from a homogeneous polyelectrolyte mixture.[15] The electrostatic interaction between PDDA and PAA was inhibited to prevent complexation before coating. The ionic complexation was restored after deposition by buffer-curing, which increases the charge density of PAA. Even though there are limited examples of

direct PEC deposition, the aforementioned buffer-cured PEC shows significant potential in reducing processing steps and achieving similar properties to LbL films. One future direction for polyelectrolyte complex coatings is the incorporation of other nanofillers. A nanofiller such as a clay nanoplatelet is a solid “polyelectrolyte”, having many surface charges that can associate with a polyelectrolyte matrix. Because of the broad scope of applications, this advancement of direct PEC deposition will hopefully lead to versatile PEC thin film systems that can be commercially scaled.

CHAPTER III

GAS BARRIER OF A POLYELECTROLYTE/CLAY COACERVATE THIN FILM*

3.1 Introduction

The PEC coacervate has viscous liqid-like properties that are suitable for quick thin-film deposition, but all-polymer coatings are sensitive to moisture.[18] In an effort to reduce the moisture sensitivity and further improve the gas barrier, clay nanoplatelets can be incorporated in the polymeric coatings.[19,20] Tsurko et al. applied PEC/clay via doctor blading and spray coating for gas barrier, [20] while another study utilized clay/ Ir(III) complex thin films for low-pressure oxygen sensing.[132] Kaolinite (KAO) clay platelets were blended into a PEC coacervate to quickly deposit a high oxygen barrier film with good moisture resistance. KAO is first dispersed in poly(acrylic acid) (PAA) solution and the resulting suspension is mixed with a polyethylenimine (PEI) solution (**Figure III-1a**). The polyelectrolyte/clay mixture undergoes liquid-liquid phase separation after annealing and slowly cooling. This coacervate is deposited on the substrate using bar-coating, as shown in **Figure III-1b**. After coating, the electrostatic interaction of the polyelectrolytes is restored by exposure to pH 4 citric acid/citrate (CA) buffer, which results in an insoluble coating. Optical transparency and oxygen barrier are further improved with humidity and heat post-treatments. Without this coating, the PET substrate has an oxygen transmission rate (OTR) of 8.6 cm^3 m^{-2} day^{-1} atm^{-1} at 0% RH and 7.2 cm^3 m^{-2} day^{-1} atm^{-1} at 80% RH. The best 4 μm thick PEC/clay coating evaluated here imparts an undetectable OTR (<

*Reprinted with permission from Chiang, H.-C.; Kolibaba, T. J.; Eberle, B.; Grunlan, J. C. Super Gas Barrier of a Polyelectrolyte/Clay Coacervate Thin Film. *Macromolecular Rapid Communications* **2021,** 42, 4.

0.005 cm^3 m^{-2} day^{-1} atm^{-1}) at 0% RH and it is 0.67 cm^3 m^{-2} day^{-1} atm^{-1} at 80% RH. This same coacervate coating also exhibits good adhesion, flexibility, and transparency.

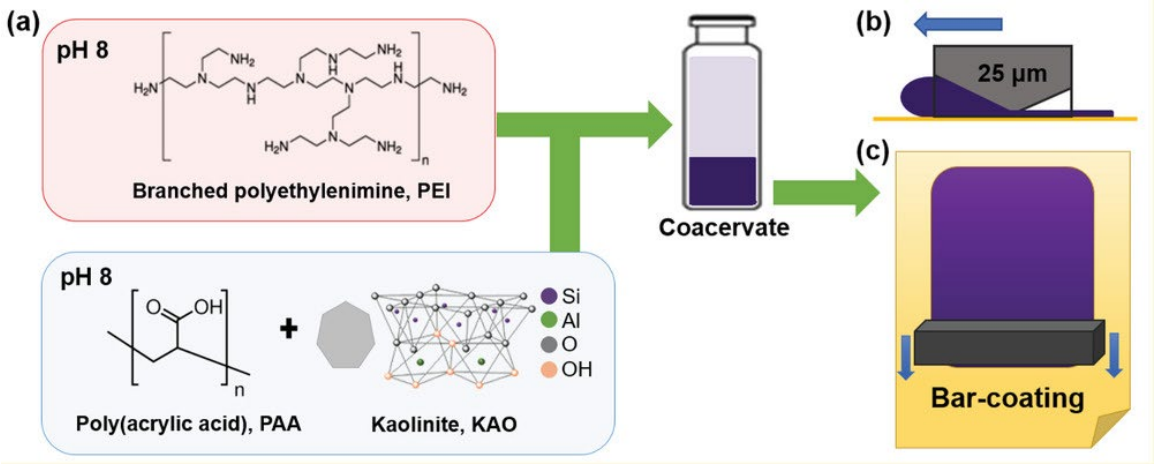

Figure III-1. Schematic of the polyelectrolyte/clay coacervate coating process. **(a)** Both PEI and PAA/KAO solutions are adjusted to pH 8 and combined into a mixture with dilute and coacervate phases. **(b)** The bar-type applicator has a gap clearance of 25 µm for the **(c)** deposition of the wet film.

3.2 Experimental

Materials : Branched polyethylenimine (PEI) (Mw 25,000 g/mol), poly (acrylic acid) (PAA) (250,000 g/mol, 35 wt % in water), kaolinite (KAO) clay, and citric acid (CA) monohydrate were purchased from Sigma-Aldrich (Milwaukee, WI). Hydrochloric acid (HCl) (ACS reagent, 37%) and sodium hydroxide (NaOH) (ACS reagent, pellets) were purchased from Sigma-Aldrich and used for solution pH adjustment. Polyethylene terephthalate (PET) film (179 µm thick) was purchased from Tekra (New Berlin, WI). 75 mm × 25 mm × 1 mm glass slides were purchased from VWR International (Radnor, PA) and used as substrates for thickness measurements.

Preparation of coacervate coating: Both PEI and PAA/KAO solutions were prepared with 18 MΩ deionized (DI) water and adjusted to pH 8. The PAA/KAO suspension was prepared by dispersing clay powder in PAA solution, followed by two rounds of tip sonication (Model VCX750; Sonics & Materials, Inc., Newtown, CT) at 15 W for 1 h each time. The polyelectrolyte/clay mixture was prepared by mixing equal volumes of the two solutions with vigorous stirring. The mixture was annealed in an oven at 70 °C for 2 h then slowly cooled down to room temperature, followed by decanting the supernatant.

Fabrication of thin films: PET film and glass slides were rinsed with DI water, methanol, and DI water. The cleaned PET was corona-treated and glass slides were plasma-treated immediately before coating. This coating suspension was deposited using the 25 μm clearance of a multiple clearance square applicator (GARDCO, Pompano Beach, FL). The coated substrate was immersed in a pH 4 200 mM CA buffer for 5 minutes, followed by DI water rinsing and filtered-air blow-drying. The humidity treatment was done by storing the film in a humid box (~95% RH) for 12 h. Heat treatment was done by hanging the film vertically in an oven at 150 °C for 2 h.

Characterization of thin films: Film thickness was measured on glass slides using a P6 profilometer (KLA–Tencor; Milpitas, CA). SEM samples were sputter-coated with 5 nm of platinum/palladium alloy before imaging with a field-emission scanning electron microscope (FESEM) (Model JSM–7500F, JEOL; Tokyo, Japan). To prepare TEM samples, coated PET was embedded into Epofix resin (EMS, Hatfield, PA), followed by curing overnight in a silicone mold. The epoxy block was cut into 90 nm thick cross-

sections using an Ultra 45° diamond knife (Diatome, Hatfield, PA). TEM images were taken using a Tecnai G2F20 TEM (FEI, Hillsboro, OR), with an accelerating voltage of 200 kV. Light transmittance was measured at 550 nm using a USB2000 UV-Vis spectrometer (Ocean Optics, Dunedin, FL). For clay content measurement, the film was scraped off the glass slide and measured using a Q–50 thermogravimetric analyzer (TA Instruments; New Castle, DE), with a heating ramp rate of 10 °C min^{-1} from room temperature to 700 °C. Oxygen transmission rate was tested by MOCON Inc. (Minneapolis, MN) using an Oxtran 2/21 ML instrument at 23 ºC under 0% RH (or 80% RH) for 120 h, in compliance with ASTM D3985. The repeatability associated with the OTR analyzer is 0.002 or 1%, whichever is greater.

3.3 Results and Discussion

Oppositely charged polyelectrolytes undergo complex coacervation when the equilibrium composition of the polymers, water, and counterions is met. This complexation is an entropically favored process due to the expulsion of small counterions and water. The salt concentration in the PEC affects the counterion release and the electrostatic interactions of the polymers.[85] This influence of salt concentration on PEI/PAA complexation has been studied by varying the concentration of sodium chloride (NaCl) in each solution before mixing.[14] The higher salt concentration (i.e. higher ionic strength), the looser associated the polyelectrolytes. When the ionic strength is high enough for both polyelectrolytes to be fully dissolved as individual chains, a truly homogeneous PEC solution is achieved. Coacervation is achieved at intermediate salt

concentration, where the polymer-rich coacervate is separated from the polymer-poor supernatant. The polyelectrolyte/clay mixture forms a coacervate when combining a pH 8 PEI solution and a pH 8 PAA/KAO suspension. The NaCl concentration of the coacervate phase is determined by instrumental neutron activation analysis (INAA). The Na and Cl concentrations are 2.02 ± 0.08 wt% and 0.91 ± 0.02 wt%, respectively. It is the use of NaOH and HCl when adjusting pH that produces these salt ions.

After removing the polymer-poor supernatant, the coacervate was applied to substrates using a hand-drawn bar-type applicator (**Figure III-1c**). The wet film thickness is determined by the 25 μm gap clearance of the applicator, which results in a 4 μm dry thickness. The as-deposited polyelectrolyte/clay film is tacky, which is likely due to the incomplete ionization of PEI at pH 8. When the amine groups of PEI are not completely protonated at pH 8, there are less positively-charged ammonium groups to ionically bond with the carboxylate groups of PAA. In order to cure the film, it was immersed in a CA buffer at pH 4 to protonate PEI. This buffer curing step improves PEI/PAA association, hence improving the durability of the film and the gas barrier due to higher cohesive energy density.[133] After curing in pH 4 buffer, the films were rinsed with deionized (DI) water to remove buffer residue and excess salt, followed by humidity treatment at 95% RH and heat treatment at 150°C.

The heat treatment can fully dry and reduce the free volume in the film, which further improves the gas barrier. These treatments produce transparent, highly conformal thin films, with average thickness of 3.61 ± 0.24 μm. The influence of the humidity treatment is revealed by scanning electron microscopy (SEM). The SEM image of the film

without humidity treatment (unhumidified) reveals considerable porosity (**Figure III-2a**), which likely arises from the fast water evaporation during drying. These pores can be eliminated by exposure to 95% RH in a humid box for 12 h. The water molecules act as a plasticizer to increase polymer mobility and fill the pores. SEM images reveal that the film with humidity treatment (humidified) has fewer pores and a smoother morphology (**Figure III-2b**). Polymer/clay composites impart gas barrier by providing a tortuous path for gas molecules wiggling around impermeable platelets.[134] A major challenge for these composite barriers is improving the clay alignment and dispersion. LbL assembly easily accomplishes this, but requires many processing steps.[8] The bar-coating process can deposit a polyelectrolyte/clay coacervate in one step with shear-induced clay alignment. Transmission electron microscopy (TEM) reveals the polymer–clay structure. The cross-sectional TEM images show a layered structure (**Figure III-2c–d**) akin to LbL assembly. The KAO platelets are aligned with the substrate, which generates high gas barrier and optical transparency.

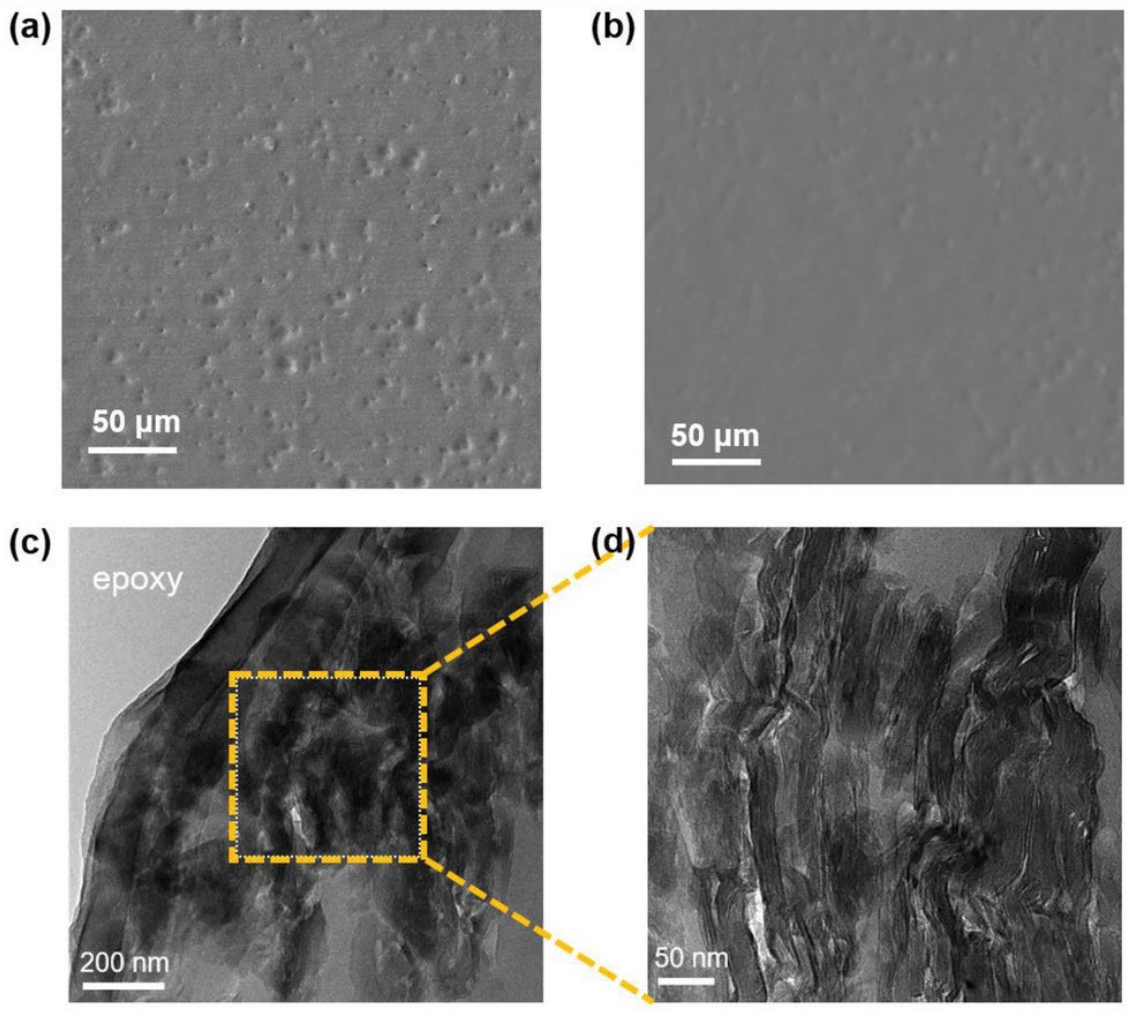

Figure III-2. Scanning electron micrographs of buffer-cured polyelectrolyte/clay film **(a)** without and **(b)** with humidity treatment. **(c,d)** Cross-sectional transmission electron micrographs show the clay alignment within the film.

The influence of clay loading was evaluated in these films by varying KAO concentration from 0.1 wt% to 2.0 wt% in the coacervate, while keeping the total solids content at 10 wt%. Light transmission through these coatings was measured by UV–Vis (**Figure III-3a**). The light transmission was normalized so uncoated 179 µm PET measured 100% at 550 nm. As the clay loading increases, the light transmission decreases

from 95.3% to 84.5%. **Figure III-3b** shows the high transparency of the polyelectrolyte/clay coated PET deposited from the highest clay loading. Oxygen barrier testing was done at 23 °C under both 0% RH and 80% RH (**Figure III-3c**). The oxygen transmission rate decreases as the clay loading increases. The highest clay loading film achieves undetectable (<0.005 cm^3 m^{-2} day^{-1} atm^{-1}) OTR at 0% RH and maintains an order of magnitude improvement over uncoated PET at 80% RH. As clay loading increases, alignment also improves due to the confinement between clay platelets. High viscosity encountered with clay loadings above 2 wt% prevent deposition of uniform films. The clay content in the final dry coatings was determined by thermogravimetric analysis. The final dry film prepared from 0.1 wt%, 1.0 wt%, and 2.0 wt% clay is estimated to have a clay content of 1.5 wt%, 21.6 wt%, and 34.4 wt%, respectively.

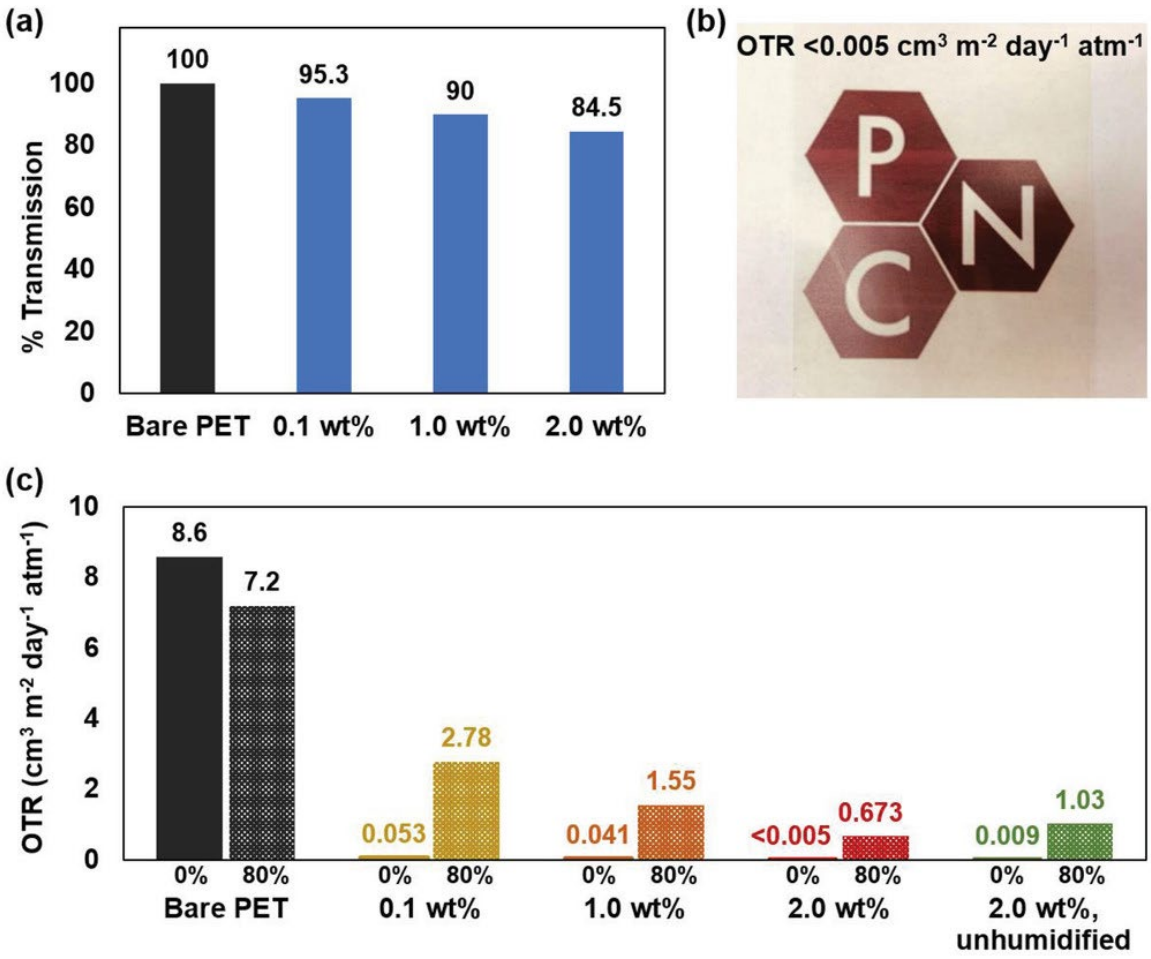

Figure III-3. (a) Light transmission of PEC/clay films measured at 550 nm as a function of the clay loading. The weight percent indicates the clay concentration in the PEC/clay mixture. **(b)** The optical image of the highest clay loading (2.0 wt% in PEC/clay mixture, equivalent to 34.4 wt% in the final dry film) reveals the high transparency of the coating. **(c)** The oxygen transmission rate of uncoated and coated 179 μm PET, with varying clay loading, measured at 23 °C under both 0% RH and 80% RH.

3.4 Conclusions

In conclusion, a polyelectrolyte/clay coacervate can be deposited as a high gas barrier layer in a single step through shear-induced clay alignment. Buffer-curing of the deposited film protonates PEI to form ionic bonds with PAA, which increases the cohesive

energy density of the film and reduces oxygen diffusion. Humidity treatment eliminates pores and generates a smoother coating. Combining humidity and heat treatment, the OTR of 179 μm PET is shown to be reduced from 8.6 to below the detection limit of commercial instrumentation (<0.005 cm^3 m^{-2} day^{-1} atm^{-1}). This coacervate coating provides PET with more than three orders of magnitude reduction in OTR, while also achieving high transparency and moisture resistance. The combination of water-based processing, ambient conditions, and quick/simple deposition make this unique coating very attractive for a variety of packaging applications.

CHAPTER IV

POLYELECTROLYTE COMPLEX THIN FILM WITH SUPER OXYGEN BAR-RIER AND HIGH MOISTURE-RESISTANCE

4.1 Introduction

Polyelectrolytes are ideal for aqueous processing, their hydrophilic nature results in moisture absorption and film swelling, which increases free volume and deteriorates gas barrier in high humidity environments.[135] Polyelectrolyte complexes with only ionic bonding are prone to lose their integrity in high humidity. Covalent crosslinking can prevent this degradation, as PEC films have been successfully crosslinked with carbodiimide,[136] bifunctional aldehydes,[137] and/or heat.[137,138] Unfortunately, improving crosslinking often requires introducing harmful chemicals or high temperature (> 120 °C). In order to improve moisture sensitivity, while avoiding harmful chemistries, the transition from a polyelectrolyte solution to a solid PEC is the key. In this study, homogeneous PEC solutions are prepared with various molar ratios of PEI:PAA, from 1:1 to 1:3, and buffer cured at pH 3 or 4 to fabricate thin films with especially strong complexation, which prevents gas diffusion and maintains high barrier under high humidity. This curing step generates ionic crosslinks between polyelectrolytes to increase the cohesive energy density of the film, which minimizes oxygen diffusion through the film.[14,15] The acid curing step was recently eliminated for a PEI/PAA coating by using volatile ammonia, which results in evaporation-induced complexation.[139]

4.2 Experimental

Materials: Branched polyethyleneimine (PEI) (Mw ~ 750,000 g/mol, 50 wt% aqueous solution) and poly(acrylic acid) (PAA) (Mw ~ 250,000 g/mol, 35 wt% aqueous solution) were purchased from Sigma-Aldrich (Milwaukee, WI) and diluted with deionized water. The chemical structures of the polyelectrolytes are shown in **Figure V-1a**. Citric acid monohydrate (CA) (98 %, Sigma-Aldrich, Milwaukee, WI) was used for preparing buffer solutions, which consist of 200 mM CA, pH adjusted to 3 or 4 with NaOH (98 %, Sigma-Aldrich, Milwaukee, WI). All solutions used were prepared using 18 MΩ deionized water. The pH of the polyelectrolyte solutions and CA buffer were adjusted using 5 M $HCl_{(aq)}$ (37 % aqueous solution, Sigma-Aldrich, Milwaukee, WI) and 5 M NaOH. 7-mil (~ 179 μm) poly(ethylene terephthalate (PET, 178 μm, ST505, Dupont-Teijin) was used as the substrate for oxygen transmission rate measurement. PET substrates were corona-treated with a BD-20C corona treater (Electro-Technic Products Inc., Chicago, IL) to impart negative surface charge, which improves the adhesion of the coating. Silicon wafers (p-type, 1 0 0, University Wafer, Boston, MA) were subjected to a plasma treatment using an Atto plasma system (Thierry, Royal Oak, MI) for 5 minutes to impart a negative surface charge before deposition. All substrates were rinsed with methanol and deionized water, followed by drying with compressed air, prior to coating deposition.

One-pot Film Assembly: The individual PEI and PAA solutions were diluted to 3 and 5 wt %, respectively. The pH of the PEI and PAA solutions was adjusted to 8 using 5 M HCl (aq) and 5 M NaOH(aq), respectively, to avoid complexation when mixing. Equal amounts by mass were added to one beaker to form the PEC mixture (4 wt% total solids),

with 1:1 PEI:PAA molar ratio (based on the molecular weight of the repeat unit). These solutions were left to mix overnight to ensure a homogeneous solution was formed. The same method was applied to prepare solutions of 1:2 and 1:3 PEI:PAA molar ratios. The general one-pot coating procedure is shown in **Figure V-1b**. The first step of the coating procedure begins by immersing the corona-treated PET substrate in the PEI:PAA solution for 5 minutes. After wicking off the extra PEC solution on the bottom of the substrate, the film was dried at 70 °C for 1 hour. These films were then cured in pH 3 or pH 4 CA buffer for 30 minutes. Cured films were then dip rinsed in three separate portions of deionized water for 30 seconds each. The final drying procedure (70 °C for 1 hour) was repeated after curing. These films were stored in a dry box before characterization. This coating process was followed identically on plasma cleaned silicon wafer substrates.

Characterization of thin films: Film characterization was done on a Si wafer with Fourier-Transform Infrared spectroscopy (FTIR), using an Alpha Platinum-ATR FTIR spectrometer (Bruker, Billerica, MA). The thickness and reduced modulus of thin films was measured on the same Si wafer with a P6 profilometer (KLA–Tencor; Milpitas, CA) and a TI 950 Triboindenter (Hysitron, Inc., Minneapolis, MN), respectively. Film surface morphology was characterized on a Si wafer with Dimension Icon atomic force microscope (AFM, Bruker, Billerica, MA) in tapping mode. Oxygen transmission rate (OTR) was tested by MOCON Inc. (Minneapolis, MN) using an Oxtran 2/21 ML instrument at 23 ºC under 0% RH or 90% RH, in compliance with ASTM D3985/F1927. The repeatability associated with the OTR analyzer is 0.002 or 1%, whichever is greater.

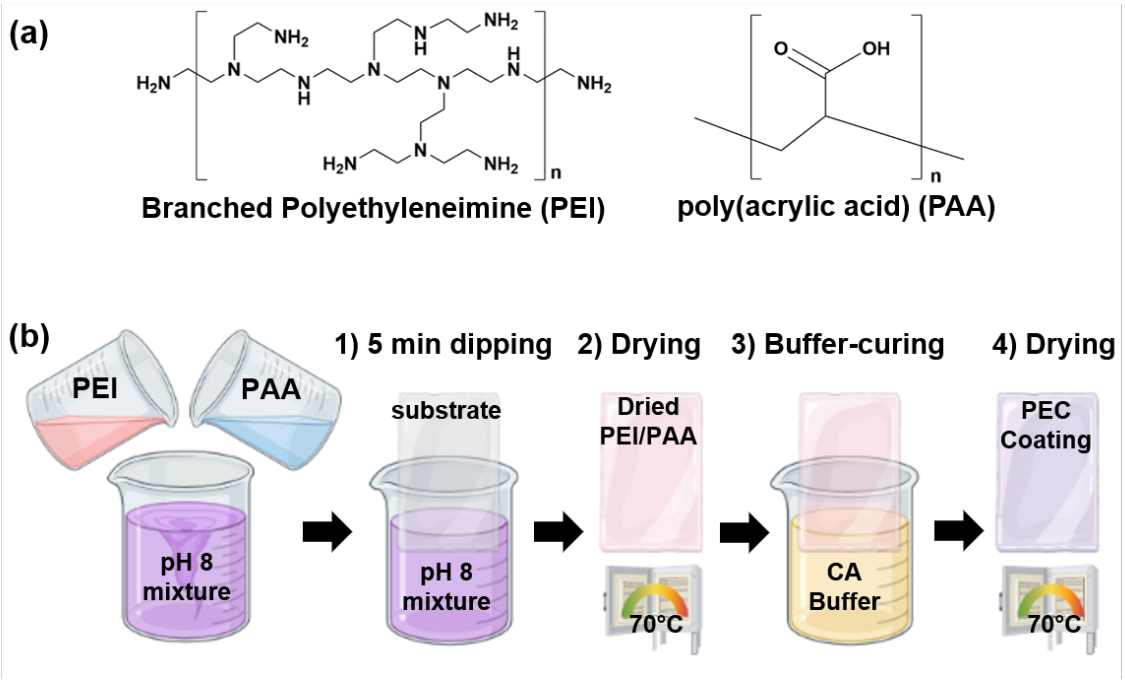

Figure IV-1. (a) Chemical structures of branched polyethyleneimine (PEI) and poly(acrylic acid) (PAA). **(b)** Schematic of the PEC dip-coating process.

4.3 Results and Discussion

Strong ionic interactions between PEI and PAA need to be inhibited to generate a stable, homogeneous coating solution. Avoiding excess electrostatic interaction prevents complexation when mixing oppositely charged polyelectrolytes, which allows simultaneous PEI/PAA deposition. Weakened interactions can be achieved by interrupting the extrinsic ion pairs (polyelectrolyte−counterion pairs) with salt addition or interrupting intrinsic ion pairs (polycation−polyanion pairs) with pH adjustment.[89] PEI and PAA are weak polyelectrolytes, which means their charge density or degree of ionization are directly affected by the pH. The pKa of the amine groups on PEI are 4.5 (primary), 6.7 (secondary), and 11.6 (tertiary),[140] while PAA has a pKa value of ~ 4.5.[141] The chemical

structures of these two polymers are shown in **Figure IV-1a**. Both polyelectrolytes are slightly charged when prepared/mixed at pH 8, where the homogeneous PEC solution can be achieved due to the lack of strong ionic interaction. This one-pot mixture was prepared with varying PEI:PAA ratios, ranging from 3:1 to 1:3, to alter the final composition of the PEC films. The PEI:PAA ratios are based on their repeat unit molar ratios, which represent the ratios of oppositely charged functional groups.

It should be noted that PEI:PAA ratios of 3:1 and 2:1 form a solid complex immediately after mixing both PEI and PAA aliquots at pH 8. Li et.al. published phase diagrams of this system, showing a similar result.[139] The solid complex (or coacervate) can be achieved with excess charged PEI at a fixed pH or with a fixed amount of PEI at a decreased pH.[142] Excess PEI causes solid complex formation, likely due to more effective ionic interaction because the branched structure of PEI has steric hindrance that prevents some amine groups from interacting. Strong complexation before thin film deposition is not desired due to the processing difficulties it creates. Only ratios of 1:1, 1:2, and 1:3 are suitable for preparing a homogeneous coating solution at pH 8. Once the one-pot PEI/PAA solution is deposited, the interrupted intrinsic ion pairs can be restored by lowering the pH with citric acid (CA) buffer immersion (i.e. buffer curing). The prepared PEI/PAA films are denoted as 1:1 PEI/PAA_3, where 1:1 represents the monomeric molar ratio of PEI:PAA and the subscript represents the CA curing pH. This coating procedure is illustrated in **Figure IV-1b**.

A The one-pot solution is deposited on the desired substrates with 5 minutes of immersion. After the initial deposition, drying at 70 °C for 1 hour immobilizes the PEC

and eliminates excess water in the film. Next, the buffer curing step triggers strong complexation by dropping the pH to 3 or 4 via immersion in a citric acid solution. PEI is highly charged at low pH (< 4) due to protonation,[143] while PAA is still charged at pH > 2,[144] which results in ionic crosslinking between these two polyelectrolytes. The strong ionic interaction between polycation and polyanion reduces free volume and oxygen permeability.[145] When the films are immersed in CA buffer at pH 5, delamination can be observed during curing and rinsing. This is likely due to the PEI not carrying enough charge density for sufficient ionic interaction. The cohesive energy of the PEC film is too low at pH > 5, so the PEI/PAA mixture has poor adhesion and is easily dissolved and rinsed off. **Figure IV-2a** compares the FTIR spectra of uncured and buffer cured PEC thin films (1:1 PEI/PAA_3). The amino groups on PEI are protonated upon exposure to CA buffer, which can strongly associate with the carboxylic acid groups and suppress N-H/O-H stretch. The broad band of the N-H/O-H stretch (~3200 cm^{-1}) of the buffer-cured PEC film is suppressed in **Figure IV-2a**, which indicates that ionic crosslinking has occurred.

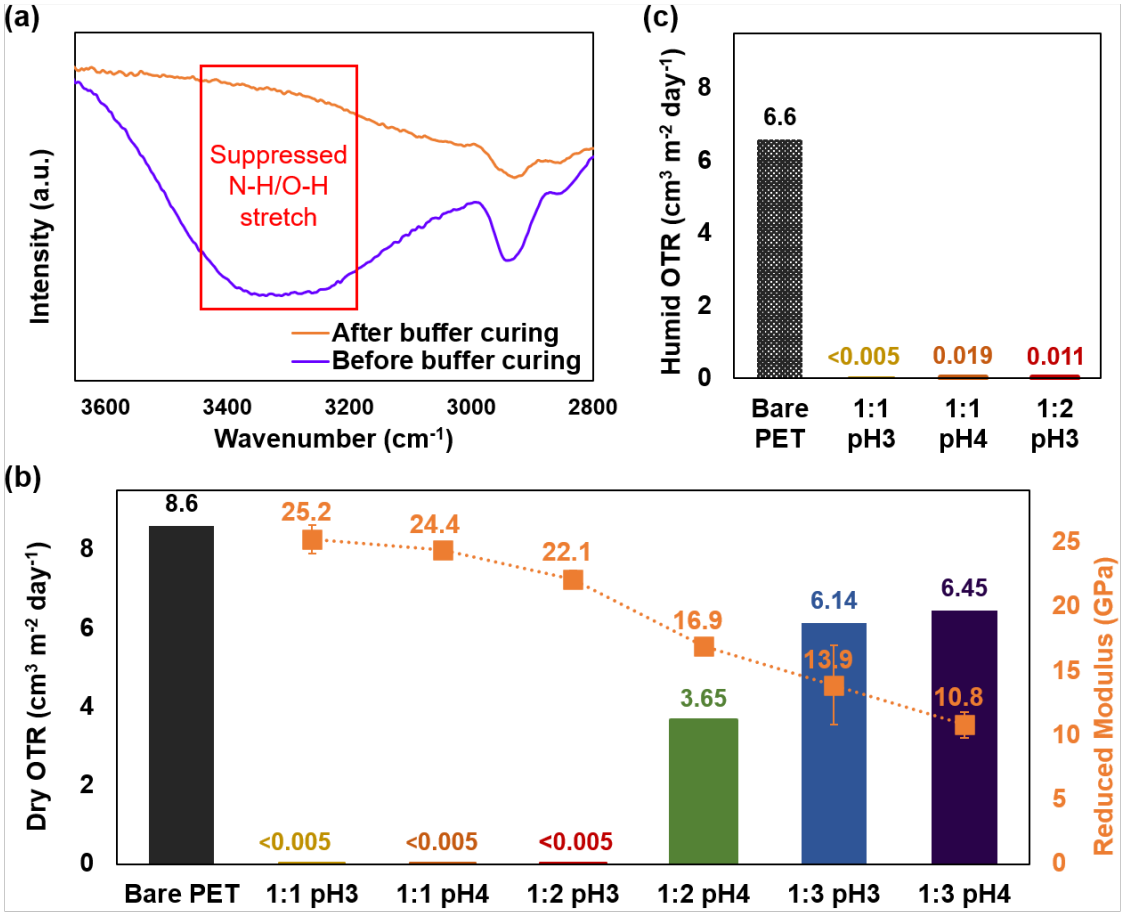

Figure IV-2. (a) FTIR spectra of the 1:1 PEC/PAA_3 film before and after buffer curing. The N-H/O-H stretch (~3200 cm^{-1}) is suppressed, suggesting ionic interaction induced by buffer-curing. **(b)** The dry oxygen transmission rate of uncoated and coated 179 µm PET, was measured at 23 °C and 0% RH. Reduced modulus was measured on a Si wafer using nanoindentation (left axis). **(c)** The humid OTR of uncoated and coated 179 µm PET, was measured at 23 °C and 90% RH.

The oxygen transmission rate (OTR) for PEC films coated on both sides of a 179 µm poly(ethylene terephthalate) (PET) sheet was measured at 23 °C under 0% RH (and 90% RH), as shown in **Figure IV-2b-c** and **Table IV-1**. The uncoated PET has a dry OTR of 8.6 and a humid OTR of 6.6 cm^3 m^{-2} day^{-1}. 1:1 PEI/PAA_3, 1:1 PEI/PAA_4, and 1:2 PEI/PAA_3 achieve undetectable (< 0.005 cm^3 m^{-2} day^{-1}) OTR at 0% RH, maintain high

barrier (< 0.02 cm^3 m^{-2} day^{-1}) at 90% RH, and have thicknesses of 859 ± 35, 959 ± 1, and 957 ± 6 nm, respectively. 1:2 PEI/PAA_4, 1:3 PEI/PAA $film_3$, and 1:3 PEI/PAA_4 did not impart high oxygen barrier and have thicknesses of 1152 ± 3, 1560 ± 14, and 740 ± 12 nm, respectively. This data is consistent with the reduced modulus (E_r) shown in **Figure IV-2b** and **Table IV-1**. The reduced elastic modulus is measured by nanoindentation, which indicates the level of cohesive energy within the PEC film. After buffer curing, the ionic crosslinking forms within the PEC film, resulting in a network that reduces film deformability (an increase of cohesive force). Greater cohesive energy not only leads to higher modulus, but also better barrier.

Higher cohesive energy can be achieved in a PEC through stronger complexation, which is controlled by molar ratio and curing pH. Although molar ratios from 1:1 to 1:3 are all able to form thin films, the 1:1 ratio performs the best in both dry and humid conditions, achieving undetectable OTR. When excess PAA is present, not all carboxylic acid groups have effective ionic interaction. This mismatch leads to a weaker ionically crosslinked network and a smaller reduced modulus. Another crucial parameter is the curing pH, which directly affects the charge density of polyelectrolytes. The degree of ionization of PEI increases as the pH decreases. The ionization of PEI was studied with titration, revealing that PEI is fully charged near pH 3 and ~ 85% charged at pH 4.[143] The films cured at pH 3 have stronger ionic interaction than pH 4 due to the higher charge density of PEI, leading to higher reduced modulus and lower OTR. Based on these results, 1:1 PEI/PAA_3 imparts the strongest complexation, which explains its excellent humid

OTR. This is one of the best barriers ever reported, achieving undetectable OTR in both dry and humid conditions, without using chemical crosslinkers or fillers.

Table IV-1. Properties of PEI/PAA films as a function of molar ratio and curing pH.

	Roughness, Rq (nm)	**Thickness (nm)**	**Reduced Modulus, Er (Gpa)**	**Dry OTR (cm^3 m^{-2} day^{-1})**	**Humid OTR (cm^3 m^{-2} day^{-1})**
1:1 PEI/PAA_3	9.6	859 ± 35	25.2 ± 1.1	< 0.005	< 0.005
1:1 PEI/PAA_4	1.5	959 ± 1	24.4 ± 0.4	< 0.005	0.019
1:2 PEI/PAA_3	4.7	957 ± 6	22.1 ± 0.7	< 0.005	0.011
1:2 PEI/PAA_4	31.3	1152 ± 3	16.9 ± 0.6	3.65	
1:3 PEI/PAA_3	36.6	1560 ± 14	13.9 ± 3.1	6.14	
1:3 PEI/PAA_4	40.8	740 ± 12	10.8 ± 1.0	6.45	

The morphology and surface roughness of PEI/PAA PEC films on silicon wafers, as functions of molar ratio and curing pH, is shown in **Figure IV-3**. These conformal coatings have smooth surfaces, with Rq less than 40 nm. The better performing films (1:1 PEI/PAA_3, 1:1 PEI/PAA_4, and 1:2 PEI/PAA_3) have smoother surfaces, with Rq less than 10 nm, while the other films (1:2 PEI/PAA_4, 1:3 PEI/PAA_3, and 1:3 PEI/PAA_4,) have slightly rougher surfaces, with Rq of 30−40 nm. The morphological changes in the latter coatings are probably due to the polymer chain rearrangement forming the ionic crosslinked structure. During the buffer curing step, the complexation occurs and forms a coalesced structure. Those films with weaker complexation (or less cohesive energy) have

excess PAA that cannot pair with charged PEI and have more free volume. The unpaired PAA is likely to have a more coiled structure, resulting in uneven distribution. The films with stronger complexation (or higher cohesive energy) do not have much excess PAA and have greater uniformity.

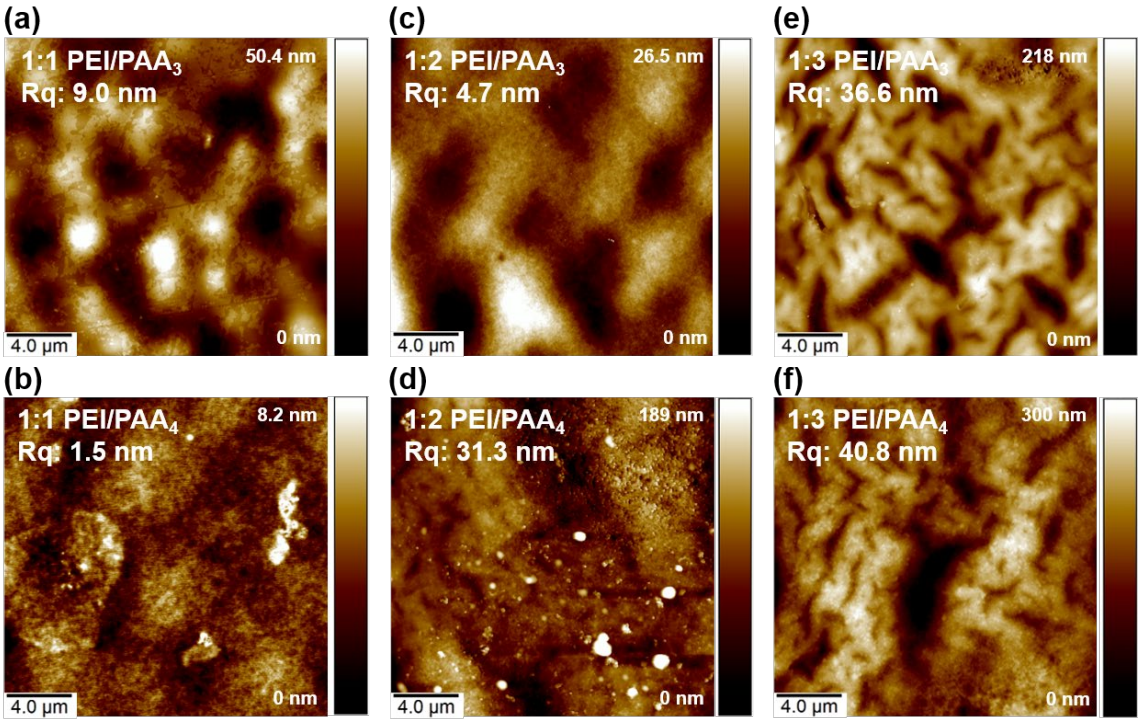

Figure IV-3. (a)−(f) Atomic force micrograph of 1:1 PEC/PAA_3, 1:1 PEC/PAA_4, 1:2 PEC/PAA_3, 1:2 PEC/PAA_4, 1:3 PEC/PAA_3, and 1:3 PEC/PAA_4 films, respectively.

4.4 Conclusions

Polyelectrolyte complex thin films of PEI and PAA can be deposited as gas barrier coatings via dip-coating, eliminating the numerous processing steps associated with layer-by-layer assembly, while maintaining very low gas transmission rate. Homogeneous PEC

solutions were prepared at pH 8 with various molar ratios to study the influence of PEC composition in the films. Curing pH was also evaluated. Films with the strongest complexation have a high reduced modulus and low OTR. The 1:1 PEI/PAA_3 coating has a thickness of 859 ± 35 nm, Er of 25.2 ± 1.1 GPa, and imparts excellent oxygen barrier (OTR < 0.005 cm^3 m^{-2} day^{-1}) in both dry and humid conditions. This is one of the best oxygen barriers ever reported, with undetectable OTR at 90% RH and without using a chemical crosslinker or fillers. This unique, water-based film is promising for various packaging applications.

CHAPTER V

EDIBLE POLYELECTROLYTE COMPLEX NANOCOATING FOR PROTECTION OF PERISHABLE PRODUCE*

5.1 Introduction

World hunger is on the rise, with 800 million people suffering from food insecurity.[146] The Food and Agriculture Organization (FAO) of the United Nations reports that approximately one-third of the food produced worldwide is wasted (i.e. never consumed), which amounts to 1.3 billion tons per year.[147] Reducing food waste is critical for combating hunger, improving food security, and reducing environmental impact (e.g. CO_2 emission). Water loss, tissue metabolism, texture deterioration, and microbial growth are the factors contributing to the loss of fresh produce.[148–150] To decelerate spoilage, food packaging is largely used to extend shelf life, but the growth of plastic waste worldwide is a counteracting issue.[151] The prevailing packaging technologies, such as metalized plastic and metal oxide thin films provide a relatively impermeable layer to oxygen, but tend to have weak adhesion, poor flexibility, poor recyclability, and require costly vacuum-based processing.[152,153] Multilayer polymeric thin films deposited from water using polyelectrolytes have shown extraordinarily low oxygen permeability and are of high interest due to better flexibility, microwavability, ease of fabrication, and better recyclability than their inorganic counterparts.[8] Due to the growing interest in

*Reprinted with permission from Chiang, H.-C.; Eberle, B.; Carlton, D.; Kolibaba, T. J.; Grunlan, J. C. Edible Polyelectrolyte Complex Nanocoating for Protection of Perishable Produce. *ACS Food Science & Technology* **2021**, 1, 495. Copyright 2022 American Chemical Society.

environmental friendliness, bio-based materials have received more attention as an alternative to synthetic polyelectrolytes. In this context, the development of greener, more cost-effective food packaging is essential to alleviating both food and plastic waste.

For food packaging, merely biodegradable or biocompatible is not enough. Edible coatings have been widely investigated to make food packaging more sustainable. Ruggeri et al. demonstrated the ability of silk fibroin and poly(vinyl alcohol) blends to create an edible coating that significantly reduces weight loss and color change of fresh-cut apples.[154] Jung et al. utilized egg-derived polymers and cellulose nanomaterials to form bio-nanocomposite coatings for perishable produce.[155] Among bio-based packing materials originating from naturally renewable resources, polysaccharides such as starch, chitosan, alginate, carrageenan, pectin, and cellulose derivatives are the most notable for the preparation of edible films.[156] In general, polysaccharides have good gas barrier properties and have wide applications in the medical and food industries.[157] Multilayered thin films of chitosan and carrageenan, deposited using the layer-by-layer assembly technique, have a high gas barrier that could be used for food packaging.[158]

In the present study, a unique edible coating, with optical transparency and high gas barrier, was prepared by coupling chitosan (CH) and pectin (PT) in a polyelectrolyte complex (PEC). Chitosan is a naturally-occurring polysaccharide that has been used in numerous applications due to its biocompatibility, biodegradability, and availability.[159,160] Chitosan is obtained by deacetylation of chitin, which is largely found in the exoskeleton of crustaceans and fungal cell walls.[161] As shown in **Figure V-1**, chitosan is a polycation that consists of β-1,4-linked d-glucosamine. Pectin is a negatively-charged

heteropolysaccharide found in plant cell walls. The composition of pectin varies, but its primary component is α-(1–4)-linked D-galacturonic acid units (**Figure V-1a**). The amine groups in chitosan and the carboxylic acid groups in pectin form a highly ionically crosslinked network upon adjusting the pH with a citric acid solution. A 1.5 µm CH/PT PEC coating on PET film exhibits an oxygen transmission rate of 0.291 cm^3 m^{-2} day^{-1} atm^{-1} and prevents the browning of apple slices for hours. This high barrier edible polyelectrolyte-pair demonstrates a unique opportunity for reducing food and plastic packaging waste.

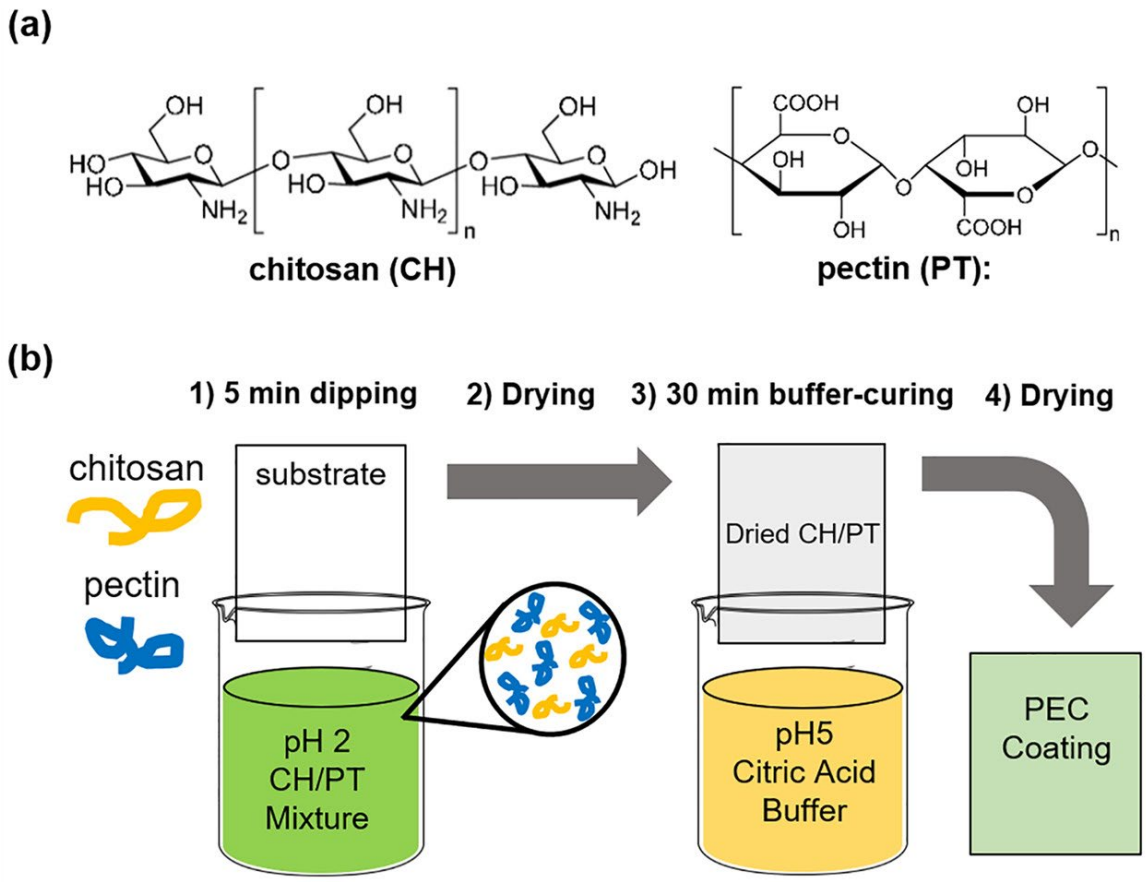

Figure V-1. (a) The chemical structure of chitosan (CH) and pectin (PT). **(b)** Schematic of the edible polyelectrolyte complex dip-coating process.

5.2 Experimental

Materials: Chitosan (item FGC-1, 95% deacetylated, 50–60 cP) was purchased from G.T.C. Union Group Ltd. (Qingdao, China). Pectin (PT, from apple, 50-75% esterification), citric acid (CA, ACS reagent), hydrochloric acid (HCl, ACS reagent, 37%), sodium hydroxide (NaOH, ACS reagent, pellets), and sodium chloride (NaCl, ACS reagent) were purchased from Sigma-Aldrich (Milwaukee, WI). All aqueous solutions were prepared in 18 MΩ Deionized (DI) water, which was also used for all rinsing procedures. Poly(ethylene terephthalate) film (PET, 179 μm thick, ST505, Dupont-Teijin) was purchased from Tekra (New Berlin, WI) and used as the substrate for oxygen transmission rate measurements.

Preparation of edible coating: A 1 wt% CH solution was prepared in 18 MΩ DI water by adjusting the pH to 1.5 using 1M HCl and stirring for 3 h. A 3 wt% PT solution was prepared in 18 MΩ DI water and rolled for at least 12 h to fully dissolve the powder. The polyelectrolyte complex (PEC) mixture was prepared by mixing equal volumes of the two solutions, rolling for at least 12 h to achieve a homogeneous solution. The final pH 2 PEC mixture (0.5 wt% CH/1.5 wt% PT) was used for dip-coating. PET film was rinsed with methanol and DI water and dried with compressed air, followed by corona-treatment immediately before coating. The coating procedure is shown in **Figure V-1b**. Substrates were immersed in the coating solution for 5 minutes, then dried at 70 °C for 5 minutes and 150 °C for 1 h (oven-dry) or dried with compressed air (blow-dry). The dried films were then cured with pH 5 200 mM CA buffer for 5 minutes, followed by DI water rinsing and the same drying procedure. Film deposition on silicon wafer (p-doped, single-side

polished from University Wafers, Boston, MA) or Au/Ti-electrode quartz crystals (Maxtek, Inc., Cypress, CA) was carried out in the same manner, except the wafer or the crystal was subjected to plasma cleaning (32G Plasma Cleaner, Harrick Plasma, Ithaca, NY) for 5 minutes instead of corona-treatment. The coating was deposited on bananas and fresh-cut apple slices using the blow-drying method.

Characterization of thin films: Fourier-transform infrared spectroscopy (FTIR) was used to compare the films on silicon wafer before and after buffer-curing using an Alpha Platinum-ATR FTIR spectrometer (Bruker, Billerica, MA). The thickness of thin films was measured on quartz crystal using a P6 profilometer (KLA–Tencor; Milpitas, CA). The coating weight was measured with a Maxtek Research Quartz Crystal Microbalance (RQCM) (Infinicon, East Syracuse, NY), with a frequency range of 3.8−6 MHz, in conjunction with 5 MHz quartz crystals. Film density was calculated using the thickness and weight data. Film surface morphology on a silicon wafer was characterized using a Dimension Icon atomic force microscope (AFM, Bruker, Billerica, MA) in tapping mode. Light transmittance through a coating deposited on PET was measured at 550 nm using a USB2000 UV-Vis spectrometer (Ocean Optics, Dunedin, FL). Light transmission was normalized by making uncoated PET 100% transmission. Oxygen transmission rate (OTR) was tested by AMETEK MOCON Inc. (Minneapolis, MN), using an Oxtran 2/21 ML instrument at 23 ºC under 0% RH, in compliance with ASTM D3985.

5.3 Results and discussion

The structure of a polyelectrolyte complex relies on the interactions between polycation and polyanion components,[16,162] whose many interfaces reduce the oxygen permeability.[137] The pKa of the amine group on chitosan is ~6.5,[163] while that of pectin is 2.8 to 4.1, so the galacturonic acid unit is negatively charged at pH values above this range.[164] When the chitosan and pectin solutions are mixed at pH 2, a homogeneous solution is formed without strong ionic interactions between the two biopolymers. In order to deposit oppositely charged polyelectrolytes simultaneously, the inhibition of electrostatic interaction is needed to prevent complexation in the solution. The CH/PT mixture can be deposited on various substrates by immersion for 5 minutes, likely adhering via van der Waals forces and dipole interactions.[15] After deposition, the coating is dried to eliminate excess water, which immobilizes the CH/PT complex. Strong ionic interaction (or complexation) is triggered by increasing the pH via buffer curing (i.e. exposure to a pH 5 citric acid buffer solution), where the carboxylic acid groups of pectin are deprotonated (i.e. become negatively-charged) and the amino groups of chitosan remain protonated (positively-charged). This highly ionically cross-linked structure imparts high gas barrier due to low free volume and high cohesion energy within the PEC.[118,145] FTIR spectroscopy was used to examine the buffer-curing of the CH/PT coating. The N-H/O-H stretch (~3200 cm^{-1}) is suppressed after curing, indicating that ionic crosslinking has occurred (**Figure V-2a**). A substantial decrease in the relative intensity of the COOH carbonyl stretch at 1736 cm^{-1} is also observed. This further suggests that the majority of the carboxylate groups are deprotonated following the buffer immersion.

The oven-dry method for the edible PEC is energy-consuming, but the coating can also be dried with blowing compressed air. Once dry, this dip-coating process results in a transparent, highly conformal thin film, with an average thickness of 574 ± 27 nm (oven-dry) or 1.480 ± 0.057 μm (blow-dry). The QCM reveals the coat weight of the edible coating is 76.85 ± 0.51 μg/cm^2 (oven-dry) or 179.75 ± 0.10 μg/cm^2 (blow-dry). The density of the oven-dried film is 1.23 ± 0.05 g/cm^3, while the density of the blow-dried film is 1.21 ± 0.04 g/cm^3. Density is independent of the method of drying, suggesting the structure of CH/PT coatings is very similar. The thinner coating of the oven-dried film is likely due to the influence of temperature that affects the viscosity of the CH/PT mixture. At higher temperature, the solution has reduced viscosity, which results in lower coat-weight.

Oxygen barrier testing was done at 23 °C under 0% RH. The oxygen transmission rate (OTR) values of the oven-dried and blow-dried films deposited on 179 μm PET are 1.51 and 0.291 cm^3 m^{-2} day^{-1} atm^{-1}, respectively (**Figure V-2b**). The oven-dried and blow-dried CH/PT films reduce the OTR of the PET by almost 6 and 30 times, respectively. Gas barrier is thickness-dependent, which accounts for the difference between the drying methods. Light transmission through these coatings was measured by UV–Vis at 550 nm and normalized with uncoated PET. The oven-dried film transmits 83.3% of light, while the blow-dried film has 79.2% light transmission. This difference in light transmission can be explained by the difference in the film thickness and surface roughness. The morphology and surface roughness of CH/PT PEC films was measured using AFM. **Figure V-2c,d** shows the topography of these coatings deposited on a silicon wafer. The

oven-dried film has a smoother surface, with R_q of 16 nm, while the blow-dried film has a rougher surface with R_q of 40 nm.

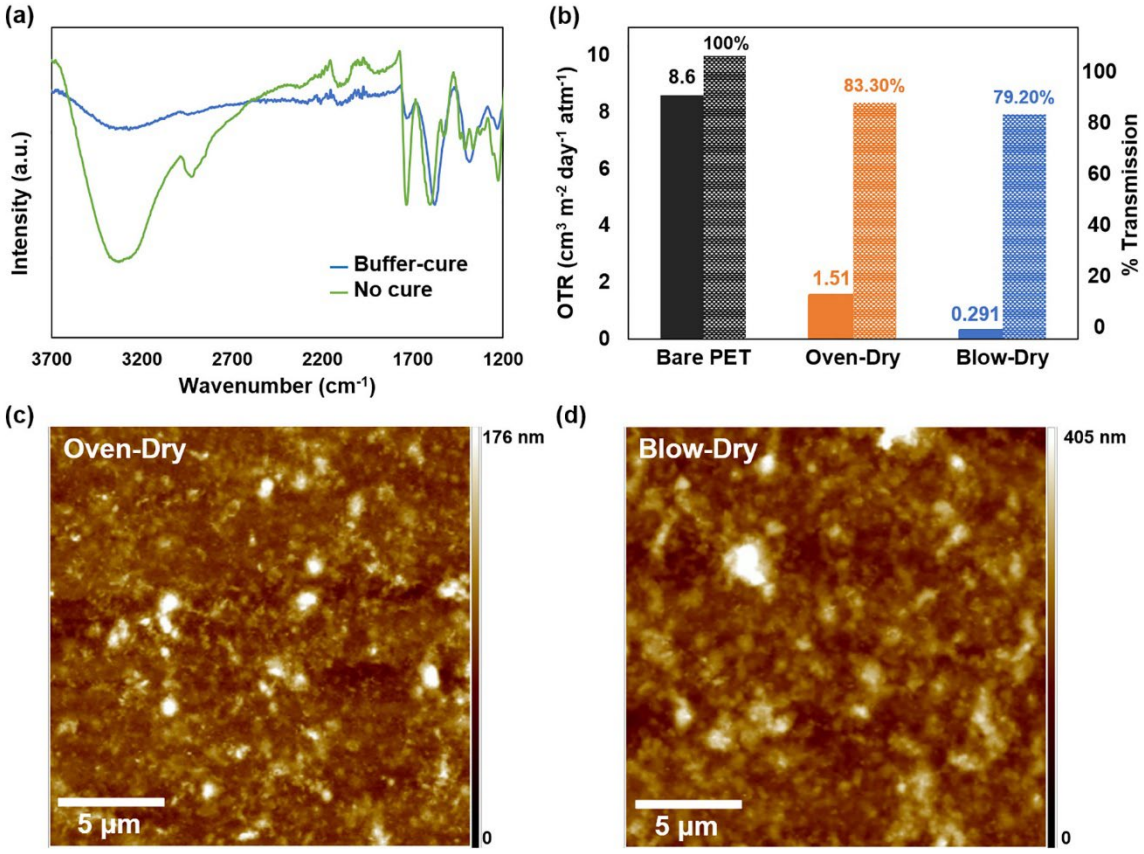

Figure V-2. (a) FTIR spectra of the CH/PT film before and after buffer-curing. These spectra have been overlaid with an arbitrary offset for clarity. The suppressed N-H/O-H stretch (~3200 cm^{-1}) indicates ionic crosslinking with buffer-curing. **(b)** The oxygen transmission rate (right axis) of uncoated and coated 179 µm PET, measured at 23 °C and 0% RH. Normalized light transmission of films measured at 550 nm (left axis). **(c)** Atomic force micrograph of oven-dried and **(d)** blow-dried CH/PT film deposited on a silicon wafer.

When this edible PEC coating is deposited on bananas (**Figure V-3a**), slower ripening is observed relative to uncoated fruit, which was dipped in DI water solutions adjusted to the same pH as the CH/PT PEC solution. The coated bananas remain green

after one week, while the uncoated bananas already exhibit brown speckles associated with spoilage. The PEC was also applied to apple slices (**Figure V-3b**), which were dipped into solutions immediately after being cut. The uncoated apple slice browned within 10 minutes, but the edible CH/PT coating prevented browning for up to three hours. This blow-dried CH/PT PEC coating has a very high oxygen barrier, with OTR of 0.291 cm^3 m^{-2} day^{-1} atm^{-1} and oxygen permeability of 1.02×10^{-18} cm^3 cm cm^{-2} s^{-1} Pa^{-1}, which is why it can effectively prevent spoilage and provides extended shelf life.

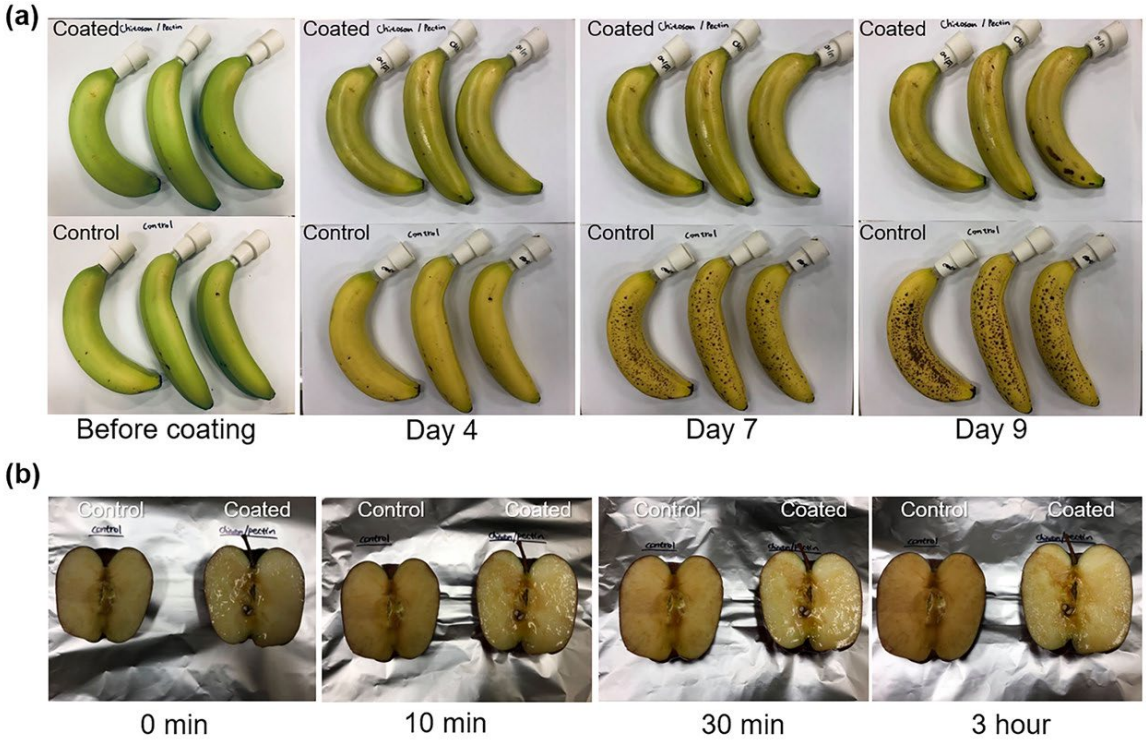

Figure V-3. (a) Comparison of CH/PT coated and uncoated banana ripening as a function of time. Bananas were aged under ambient conditions. **(b)** Comparison of CH/PT coated and uncoated apple browning as a function of time under ambient conditions.

5.4 Conclusions

A protective coating for fruit was prepared from a polyelectrolyte complex of chitosan as polycation and pectin as polyanion. This edible coating was deposited via dip-coating, followed by oven or blow drying and buffer-curing with citric acid solution. The blow-dried film imparts a low OTR of 0.291 cm^3 m^{-2} day^{-1} atm^{-1}, while retaining 79.2% light transmission, with a thickness of only 1.5 μm. With an oxygen permeability of 1.02×10^{-18} cm^3 cm cm^{-2} s^{-1} Pa^{-1}, this is one of the best barriers ever reported using only generally-recognized-as-safe (GRAS) polymers. When deposited on perishable fruits, this imperceptible protective layer slows the ripening of bananas and browning of apple slices. These results suggest that an edible CH/PT PEC coating could be useful for extending the shelf life of perishable produce, reducing food and plastic packaging waste.

CHAPTER VI

CONCLUSIONS AND FUTURE WORK

6.1 New and Improved Developments for Polyelectrolyte Complex Gas Barrier Thin Films

This dissertation is focused on improvements in one-pot PEC gas barrier thin films. These improvements generate polymeric gas barrier coatings with fewer processing steps and moisture resistance. By incorporating aligned clay platelets into the PEC matrix, a PEC/clay gas barrier system is shown to impart high barrier with high transparency and moisture resistance. This one-pot PEC solution is deposited with optimized composition and curing pH to achieve super oxygen barrier with high reduced modulus and high moisture resistance. A similar strategy is applied to a polysaccharide-based PEC to deposit an edible gas barrier thin film. These new and improved PEC thin films have shown great potential in gas barrier applications.

6.1.1 Super Gas Barrier of a Polyelectrolyte/Clay Coacervate Thin Film

Chapter III shows that a polyelectrolyte/clay coacervate composed of PEI, PAA, and kaolinite clay (KAO) can be deposited in a single step, followed by humidity and thermal post-treatments. When deposited onto a 179 μm PET substrate, a 4 μm coacervate coating reduces the OTR by more than three orders of magnitude, while maintaining high transparency. This single-step deposition process uses only low-cost, water-based components and ambient conditions, which could be used for sensitive food and electronics packaging.

6.1.2 Polyelectrolyte Complex with Super Oxygen Barrier and High Moisture-Resistance

Chapter IV describes a system of various molar ratios (1:1, 1:2, and 1:3) of PEI and PAA as one-pot coating solutions, which can be deposited via a simple dip-coating process and cured with a citric acid buffer solution. As-prepared conformal thin films impart excellent gas barrier, high modulus, and high moisture resistance. Undetectable OTR, at both 0 % and 90% RH, can be achieved with a PEI:PAA molar ratio of 1:1 and buffer curing at pH 3. The strong complexation from ionic crosslinking creates an unusually dense thin film that is promising for various packaging applications (food, electronics, etc.). This thin film exhibits one of the best ever polymer-based oxygen barriers at high humidity.

6.1.3 Edible Polyelectrolyte Complex Nanocoating for Protection of Perishable Produce

An edible polysaccharide-based PEC gas barrier thin film is demonstrated in Chapter V. This edible PEC consisting of chitosan and pectin are deposited onto fresh fruit to extend shelf life. This unique edible coating imparts high gas barrier and high transparency that can slow the ripening of bananas and browning of apple slices. A 1.5 μm thick chitosan/pectin coating reduces the oxygen transmission rate of 179 μm polyester film by more than ten times. This single-step deposition process uses only water-soluble, edible biopolymers and ambient conditions, which is promising for reducing both food and packaging waste.

6.2 Future Directions

6.2.1. Diels-Alder Based Self-Healing Coating

Crosslinking thin films is a promising solution to reduce moisture sensitivity but once the crosslinked covalent networks are damaged, the desired properties will be lost. The ability to self-heal after damaging, and restore desirable properties, is important for polymer composites. A self-healing PEI/PAA coating has been investigated,[165] but it requires high humidity and is not suitable for applications susceptible to moisture. Reversible Diel-Alder reaction can be utilized to prepare self-healable polymer composites.[166,167] This reaction, also known as [4+2] cycloaddition, provides excellent control of stereochemistry in synthetic organic chemistry. It involves the combination of a diene with an alkene (acting as a dienophile) and requires low energy to form a cyclohexane derivative. In general, to improve the yields in the Diels-Alder reaction, substitution with groups of opposite polarity is needed. An electron-rich diene and an electron-poor dienophile can form more stable cyclohexenes with better yields. The majority of examples reported employ electron-withdrawing groups on the dienophile and electron-donating groups on the diene, with furan-maleimide being the best known.[168] One attractive feature of furan-maleimide is that reversibility can be controlled simply with temperature (i.e. no metal catalyst or organic solvent is needed). To self-repair after partial internal damage, the covalent polymer network can be disintegrated by simply heating, followed by reforming the network structure under room temperature.

A PEC incorporating furan-maleimide-based Diels-Alder reaction to the polymer chain and linker is proposed. The amine group on PEI can react with the aldehyde moiety on furfural to form an imine as shown in **Figure VI-1**. This synthesis can be monitored with NMR to verify that modification has occurred. Next, this furan functionalized PEI will be mixed with PAA and a stoichiometric amount of bismaleimide at room temperature. These steps should result in a thermally reversible PEC matrix, as shown in **Figure VI-2**.

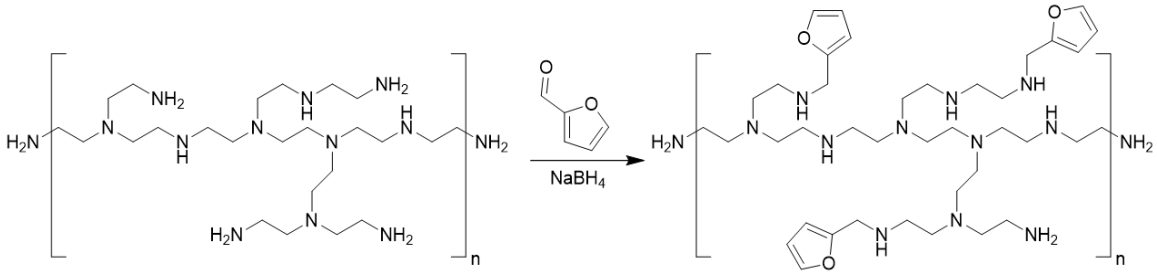

Figure VI-1. Scheme of furfural modification. The amine group on PEI can react with the aldehyde moiety on furfural to form imine with a furan moiety.

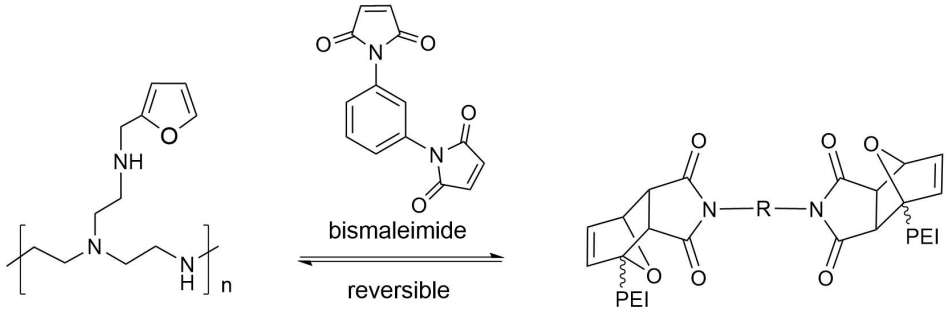

Figure VI-2. Scheme of furan-maleimide based Diel-Alder reaction. Bismaleimide is the molecule used to crosslink modified PEI to form a thermal reversable covalent network.

Micro-cracks will be created in the coating by extension to test self-healing. Self-healing will be initiated by heating the film to 150 °C, then cooling down to room temperature. Scanning electron microscope surface images can verify the self-healing before and after the heat treatment. OTR measurements will also be conducted before and after the heat treatment to confirm the self-healing. The successful PEI modification and film deposition, with good OTR before and after self-healing, will demonstrate the durability of this unique PEC gas barrier film.

6.2.2 Chitosan/Gelatin Edible Gas Barrier Thin Film Crosslinked by Riboflavin

The hydrophilic nature of biopolymers results in moisture absorption, which increases free volume and decreases gas barrier. Electrostatic assemblies, with only ionic bonding, are prone to lose their integrity in high humidity environments. Covalent crosslinking is an effective approach to prevent this degradation by creating more robust and densely-packed molecular organization. PEC films have been successfully crosslinked with carbodiimide,[136] bifunctional aldehydes,[138] and/or heat.[138,169]

In order to create edible coatings with reduced moisture sensitivity, an edible crosslinker is needed. Riboflavin, also known as vitamin B2, is a water-soluble nutrient present in eggs and vegetables. Riboflavin is photoactive due to its heterocyclic isoalloxazine moiety and has maximum absorption at 365 and 445 nm.[170] In the photosensitization, riboflavin is excited to a short lived singlet state, which decays to the highly reactive and long-lived triplet-excited state.[171] The triplet excited state is a powerful

oxidant that produces singlet oxygen. The singlet oxygen and riboflavin radicals can initiate further oxidation via both radical and non-radical reactions, which results in the desired crosslink in the polymer network. Based on this mechanism, riboflavin crosslinking has been used in corneal surgery to crosslink corneal collagen.[172] A previous study indicates that tyrosine probably contributes to the riboflavin crosslinking of collagen through the formation of dityrosine.[173]

In this proposal, chitosan and gelatin would be used to prepare a PEC suspension for dip-coating. Gelatin is a polypeptide derived from collagen taken from animal body parts. In order to achieve a stable chitosan/gelatin PEC solution without strong complexation, the pH of this film forming solution will be evaluated. The pH should be adjusted below 6.2 to prevent chitosan precipitation. The isoelectric point (pI) of gelatin is pH 4.5-5.2, where all the gelatin chains are neutral. This is a good pH range to get intermediate polyelectrolyte complexation. After the PEC solution without solid precipitation is achieved, riboflavin will be blended in for later photocrosslinking. Edible coatings will be prepared with photocrosslinking performed with 365nm UV light exposure. Further investigation is required to verify the ionic bonding between chitosan and gelatin, and riboflavin crosslinking, by using FTIR. Swelling can be used to quickly screen the crosslinking conditions and OTR will be measured before and after the photocrosslinking under high humidity to verify the improvement of moisture resistance.

REFERENCES

(1) Lange, J.; Wyser, Y. Recent Innovations in Barrier Technologies for Plastic Packaging—a Review. *Packaging Technology and Science* **2003**, *16* (4), 149–158. https://doi.org/10.1002/pts.621.

(2) Graff, G. L.; Burrows, P. E.; Williford, R. E.; Praino, R. F. Barrier Layer Technology for Flexible Displays. In *Flexible Flat Panel Displays*; John Wiley & Sons, Ltd, 2005; pp 57–77. https://doi.org/10.1002/0470870508.ch4.

(3) Han, J.-W.; Ruiz-Garcia, L.; Qian, J.-P.; Yang, X.-T. Food Packaging: A Comprehensive Review and Future Trends. *Comprehensive Reviews in Food Science and Food Safety* **2018**, *17* (4), 860–877. https://doi.org/10.1111/1541-4337.12343.

(4) Goulas, A. E. Overall Migration from Commercial Coextruded Food Packaging Multilayer Films and Plastics Containers into Official EU Food Simulants. *Eur Food Res Technol* **2001**, *212* (5), 597–602. https://doi.org/10.1007/s002170000294.

(5) Marsh, K.; Bugusu, B. Food Packaging—Roles, Materials, and Environmental Issues. *Journal of Food Science* **2007**, *72* (3), R39–R55. https://doi.org/10.1111/j.1750-3841.2007.00301.x.

(6) Roberts, A. P.; Henry, B. M.; Sutton, A. P.; Grovenor, C. R. M.; Briggs, G. A. D.; Miyamoto, T.; Kano, M.; Tsukahara, Y.; Yanaka, M. Gas Permeation in Silicon-Oxide/Polymer (SiOx/PET) Barrier Films: Role of the Oxide Lattice, Nano-Defects and Macro-Defects. *Journal of Membrane Science* **2002**, *208* (1), 75–88. https://doi.org/10.1016/S0376-7388(02)00178-3.

(7) Jarvis, K. L.; Evans, P. J. Growth of Thin Barrier Films on Flexible Polymer Substrates by Atomic Layer Deposition. *Thin Solid Films* **2017**, *624*, 111–135. https://doi.org/10.1016/j.tsf.2016.12.055.

(8) Priolo, M. A.; Holder, K. M.; Guin, T.; Grunlan, J. C. Recent Advances in Gas Barrier Thin Films via Layer-by-Layer Assembly of Polymers and Platelets. *Macromolecular Rapid Communications* **2015**, *36* (10), 866–879. https://doi.org/10.1002/marc.201500055.

(9) Tan, B.; Thomas, N. L. A Review of the Water Barrier Properties of Polymer/Clay and Polymer/Graphene Nanocomposites. *Journal of Membrane Science* **2016**, *514*, 595–612. https://doi.org/10.1016/j.memsci.2016.05.026.

(10) *Food and Beverage Packaging Technology, 2nd Edition | Wiley*. Wiley.com. https://www.wiley.com/en-us/Food+and+Beverage+Packaging+Technology%2C+2nd+Edition-p-9781444392173 (accessed 2020-04-09).

(11) Priolo, M. A.; Gamboa, D.; Grunlan, J. C. Transparent Clay−Polymer Nano Brick Wall Assemblies with Tailorable Oxygen Barrier. *ACS Appl. Mater. Interfaces* **2010**, *2* (1), 312–320. https://doi.org/10.1021/am900820k.

(12) Richardson, J. J.; Cui, J.; Björnmalm, M.; Braunger, J. A.; Ejima, H.; Caruso, F. Innovation in Layer-by-Layer Assembly. *Chem. Rev.* **2016**, *116* (23), 14828–14867. https://doi.org/10.1021/acs.chemrev.6b00627.

(13) Ariga, K.; Yamauchi, Y.; Rydzek, G.; Ji, Q.; Yonamine, Y.; Wu, K. C.-W.; Hill, J. P. Layer-by-Layer Nanoarchitectonics: Invention, Innovation, and Evolution. *Chem. Lett.* **2013**, *43* (1), 36–68. https://doi.org/10.1246/cl.130987.

(14) Haile, M.; Sarwar, O.; Henderson, R.; Smith, R.; Grunlan, J. C. Polyelectrolyte Coacervates Deposited as High Gas Barrier Thin Films. *Macromol. Rapid Commun.* **2017**, *38* (1), 1600594. https://doi.org/10.1002/marc.201600594.

(15) Smith, R. J.; Long, C. T.; Grunlan, J. C. Transparent Polyelectrolyte Complex Thin Films with Ultralow Oxygen Transmission Rate. *Langmuir* **2018**, *34* (37), 11086–11091. https://doi.org/10.1021/acs.langmuir.8b02391.

(16) Wang, Q.; Schlenoff, J. B. The Polyelectrolyte Complex/Coacervate Continuum. *Macromolecules* **2014**, *47* (9), 3108–3116. https://doi.org/10.1021/ma500500q.

(17) Sing, C. E.; Perry, S. L. Recent Progress in the Science of Complex Coacervation. *Soft Matter* **2020**, *16* (12), 2885–2914. https://doi.org/10.1039/D0SM00001A.

(18) Kurek, M.; Ščetar, M.; Voilley, A.; Galić, K.; Debeaufort, F. Barrier Properties of Chitosan Coated Polyethylene. *Journal of Membrane Science* **2012**, *403–404*, 162–168. https://doi.org/10.1016/j.memsci.2012.02.037.

(19) Priolo, M. A.; Holder, K. M.; Greenlee, S. M.; Grunlan, J. C. Transparency, Gas Barrier, and Moisture Resistance of Large-Aspect-Ratio Vermiculite Nanobrick Wall Thin Films. *ACS Appl. Mater. Interfaces* **2012**, *4* (10), 5529–5533. https://doi.org/10.1021/am3014289.

(20) Tsurko, E. S.; Feicht, P.; Nehm, F.; Ament, K.; Rosenfeldt, S.; Pietsch, I.; Roschmann, K.; Kalo, H.; Breu, J. Large Scale Self-Assembly of Smectic Nanocomposite Films by Doctor Blading versus Spray Coating: Impact of Crystal Quality on Barrier Properties. *Macromolecules* **2017**, *50* (11), 4344–4350. https://doi.org/10.1021/acs.macromol.7b00701.

(21) Mkandawire, M.; Aryee, A. N. Resurfacing and Modernization of Edible Packaging Material Technology. *Current Opinion in Food Science* **2018**, *19*, 104–112. https://doi.org/10.1016/j.cofs.2018.03.010.

(22) Patel, A. R. Functional and Engineered Colloids from Edible Materials for Emerging Applications in Designing the Food of the Future. *Advanced Functional Materials* **2020**, *30* (18), 1806809. https://doi.org/10.1002/adfm.201806809.

(23) Tao, H.; Brenckle, M. A.; Yang, M.; Zhang, J.; Liu, M.; Siebert, S. M.; Averitt, R. D.; Mannoor, M. S.; McAlpine, M. C.; Rogers, J. A.; Kaplan, D. L.; Omenetto, F. G. Silk-Based Conformal, Adhesive, Edible Food Sensors. *Advanced Materials* **2012**, *24* (8), 1067–1072. https://doi.org/10.1002/adma.201103814.

(24) Siracusa, V.; Rocculi, P.; Romani, S.; Rosa, M. D. Biodegradable Polymers for Food Packaging: A Review. *Trends in Food Science & Technology* **2008**, *19* (12), 634–643. https://doi.org/10.1016/j.tifs.2008.07.003.

(25) Dou, Y.; Pan, T.; Xu, S.; Yan, H.; Han, J.; Wei, M.; Evans, D. G.; Duan, X. Transparent, Ultrahigh-Gas-Barrier Films with a Brick–Mortar–Sand Structure. *Angewandte Chemie International Edition* **2015**, *54* (33), 9673–9678. https://doi.org/10.1002/anie.201503797.

(26) Affinito, J. D.; Gross, M. E.; Coronado, C. A.; Graff, G. L.; Greenwell, I. N.; Martin, P. M. A New Method for Fabricating Transparent Barrier Layers. *Thin Solid Films* **1996**, *290–291*, 63–67. https://doi.org/10.1016/S0040-6090(96)09202-4.

(27) Inagaki, N.; Tasaka, S.; Nakajima, T. Preparation of Oxygen Gas Barrier Polypropylene Films by Deposition of SiOx Films Plasma-Polymerized from Mixture of Tetramethoxysilane and Oxygen. *Journal of Applied Polymer Science* **2000**, *78* (13), 2389–2397. https://doi.org/10.1002/1097-4628(20001220)78:13<2389::AID-APP160>3.0.CO;2-J.

(28) Burrows, P. E.; Graff, G. L.; Gross, M. E.; Martin, P. M.; Shi, M. K.; Hall, M.; Mast, E.; Bonham, C.; Bennett, W.; Sullivan, M. B. Ultra Barrier Flexible Substrates for Flat Panel Displays. *Displays* **2001**, *22* (2), 65–69. https://doi.org/10.1016/S0141-9382(00)00064-0.

(29) Cui, Y.; Kumar, S.; Kona, B. R.; Houcke, D. van. Gas Barrier Properties of Polymer/Clay Nanocomposites. *RSC Adv.* **2015**, *5* (78), 63669–63690. https://doi.org/10.1039/C5RA10333A.

(30) Langowski, H.-C. Permeation of Gases and Condensable Substances through Monolayer and Multilayer Structures. In *Plastic Packaging*; John Wiley & Sons, Ltd, 2008; pp 297–347. https://doi.org/10.1002/9783527621422.ch10.

(31) Yalcin, B.; Cakmak, M. Polymer Film Substrates for Roll-to-Roll Manufacturing. In *Roll-to-Roll Manufacturing*; John Wiley & Sons, Ltd, 2018; pp 171–224. https://doi.org/10.1002/9781119163824.ch6.

(32) Chatham, H. Oxygen Diffusion Barrier Properties of Transparent Oxide Coatings on Polymeric Substrates. *Surface and Coatings Technology* **1996**, *78* (1), 1–9. https://doi.org/10.1016/0257-8972(95)02420-4.

(33) Quintino, L. 1 - Overview of Coating Technologies. In *Surface Modification by Solid State Processing*; Miranda, R., Ed.; Woodhead Publishing, 2014; pp 1–24. https://doi.org/10.1533/9780857094698.1.

(34) Li, Y.; Zhao, C. 8 - Advanced Interconnect Technology and Reliability. In *CMOS Past, Present and Future*; Radamson, H. H., Luo, J., Simoen, E., Zhao, C., Eds.; Woodhead Publishing Series in Electronic and Optical Materials; Woodhead Publishing, 2018; pp 215–247. https://doi.org/10.1016/B978-0-08-102139-2.00008-2.

(35) Adamov, M.; Perović, B.; Nenadović, T. Electrical and Structural Properties of Thin Gold Films Obtained by Vacuum Evaporation and Sputtering. *Thin Solid Films* **1974**, *24* (1), 89–100. https://doi.org/10.1016/0040-6090(74)90254-5.

(36) Mattox, D. M. Chapter 8 - Arc Vapor Deposition. In *Handbook of Physical Vapor Deposition (PVD) Processing (Second Edition)*; Mattox, D. M., Ed.; William Andrew Publishing: Boston, 2010; pp 287–300. https://doi.org/10.1016/B978-0-8155-2037-5.00008-3.

(37) Jamieson, E. H. H.; Windle, A. H. Structure and Oxygen-Barrier Properties of Metallized Polymer Film. *J Mater Sci* **1983**, *18* (1), 64–80. https://doi.org/10.1007/BF00543811.

(38) Treutlein, R.; Bergsmann, M.; Stonley, C. J. Reel-to-Reel Vacuum Metallization. In *Organic Electronics*; John Wiley & Sons, Ltd, 2006; pp 181–202. https://doi.org/10.1002/3527608753.ch8.

(39) Felts, J. T. Transparent Barrier Coatings Update: Flexible Substrates. *Journal of Plastic Film & Sheeting* **1993**, *9* (2), 139–158. https://doi.org/10.1177/875608799300900206.

(40) Knappich, F.; Schlummer, M.; Mäurer, A.; Prestel, H. A New Approach to Metal- and Polymer-Recovery from Metallized Plastic Waste Using Mechanical Treatment and Subcritical Solvents. *J Mater Cycles Waste Manag* **2018**, *20* (3), 1541–1552. https://doi.org/10.1007/s10163-018-0717-6.

(41) Walker, M.; Meermann, F.; Schneider, J.; Bazzoun, K.; Feichtinger, J.; Schulz, A.; Krüger, J.; Schumacher, U. Investigations of Plasma Polymerized Barrier Films on Polymeric Materials. *Surface and Coatings Technology* **2005**, *200* (1), 947–952. https://doi.org/10.1016/j.surfcoat.2005.02.135.

(42) Erlat, A. G.; Spontak, R. J.; Clarke, R. P.; Robinson, T. C.; Haaland, P. D.; Tropsha, Y.; Harvey, N. G.; Vogler, E. A. SiOx Gas Barrier Coatings on Polymer Substrates: Morphology and Gas Transport Considerations. *J. Phys. Chem. B* **1999**, *103* (29), 6047–6055. https://doi.org/10.1021/jp990737e.

(43) da Silva Sobrinho, A. S.; Czeremuszkin, G.; Latrèche, M.; Dennler, G.; Wertheimer, M. R. A Study of Defects in Ultra-Thin Transparent Coatings on Polymers. *Surface and Coatings Technology* **1999**, *116–119*, 1204–1210. https://doi.org/10.1016/S0257-8972(99)00152-8.

(44) Leterrier, Y. Durability of Nanosized Oxygen-Barrier Coatings on Polymers. *Progress in Materials Science* **2003**, *48* (1), 1–55. https://doi.org/10.1016/S0079-6425(02)00002-6.

(45) Freeman, B. D. Basis of Permeability/Selectivity Tradeoff Relations in Polymeric Gas Separation Membranes. *Macromolecules* **1999**, *32* (2), 375–380. https://doi.org/10.1021/ma9814548.

(46) Choudalakis, G.; Gotsis, A. D. Permeability of Polymer/Clay Nanocomposites: A Review. *European Polymer Journal* **2009**, *45* (4), 967–984. https://doi.org/10.1016/j.eurpolymj.2009.01.027.

(47) Lee, W. M. Selection of Barrier Materials from Molecular Structure. *Polymer Engineering & Science* **1980**, *20* (1), 65–69. https://doi.org/10.1002/pen.760200111.

(48) Pavlidou, S.; Papaspyrides, C. D. A Review on Polymer–Layered Silicate Nanocomposites. *Progress in Polymer Science* **2008**, *33* (12), 1119–1198. https://doi.org/10.1016/j.progpolymsci.2008.07.008.

(49) Kango, S.; Kalia, S.; Celli, A.; Njuguna, J.; Habibi, Y.; Kumar, R. Surface Modification of Inorganic Nanoparticles for Development of Organic–Inorganic Nanocomposites—A Review. *Progress in Polymer Science* **2013**, *38* (8), 1232–1261. https://doi.org/10.1016/j.progpolymsci.2013.02.003.

(50) Anglin, E. J.; Cheng, L.; Freeman, W. R.; Sailor, M. J. Porous Silicon in Drug Delivery Devices and Materials. *Advanced Drug Delivery Reviews* **2008**, *60* (11), 1266–1277. https://doi.org/10.1016/j.addr.2008.03.017.

(51) Chen, M.-C.; Mi, F.-L.; Liao, Z.-X.; Hsiao, C.-W.; Sonaje, K.; Chung, M.-F.; Hsu, L.-W.; Sung, H.-W. Recent Advances in Chitosan-Based Nanoparticles for Oral Delivery of Macromolecules. *Adv Drug Deliv Rev* **2013**, *65* (6), 865–879. https://doi.org/10.1016/j.addr.2012.10.010.

(52) Smith, R. J.; Moule, M. G.; Leon, P. A.; Iverson, E. T.; Kolibaba, T. J.; Cirillo, J. D.; Grunlan, J. C. Polyelectrolyte Complex That Minimizes Bacterial Adhesion to Polyester. *Macromolecular Materials and Engineering* **2021**, *306* (12), 2100579. https://doi.org/10.1002/mame.202100579.

(53) Arora, A.; Padua, G. W. Review: Nanocomposites in Food Packaging. *Journal of Food Science* **2010**, *75* (1), R43–R49. https://doi.org/10.1111/j.1750-3841.2009.01456.x.

(54) Okada, A.; Usuki, A. Twenty Years of Polymer-Clay Nanocomposites. *Macromolecular Materials and Engineering* **2006**, *291* (12), 1449–1476. https://doi.org/10.1002/mame.200600260.

(55) Vaia, R. A.; Giannelis, E. P. Liquid Crystal Polymer Nanocomposites: Direct Intercalation of Thermotropic Liquid Crystalline Polymers into Layered Silicates. *Polymer* **2001**, *42* (3), 1281–1285. https://doi.org/10.1016/S0032-3861(00)00508-5.

(56) Jagadale, T. C.; Takale, S. P.; Sonawane, R. S.; Joshi, H. M.; Patil, S. I.; Kale, B. B.; Ogale, S. B. N-Doped TiO2 Nanoparticle Based Visible Light Photocatalyst by Modified Peroxide Sol−Gel Method. *J. Phys. Chem. C* **2008**, *112* (37), 14595–14602. https://doi.org/10.1021/jp803567f.

(57) Haes, A. J.; Van Duyne, R. P. A Nanoscale Optical Biosensor: Sensitivity and Selectivity of an Approach Based on the Localized Surface Plasmon Resonance Spectroscopy of Triangular Silver Nanoparticles. *J. Am. Chem. Soc.* **2002**, *124* (35), 10596–10604. https://doi.org/10.1021/ja020393x.

(58) Fu, X.; Qutubuddin, S. Polymer–Clay Nanocomposites: Exfoliation of Organophilic Montmorillonite Nanolayers in Polystyrene. *Polymer* **2001**, *42* (2), 807–813. https://doi.org/10.1016/S0032-3861(00)00385-2.

(59) Sun, X.; Huang, C.; Wang, L.; Liang, L.; Cheng, Y.; Fei, W.; Li, Y. Recent Progress in Graphene/Polymer Nanocomposites. *Advanced Materials* **2021**, *33* (6), 2001105. https://doi.org/10.1002/adma.202001105.

(60) Azeredo, H. M. C. de. Nanocomposites for Food Packaging Applications. *Food Research International* **2009**, *42* (9), 1240–1253. https://doi.org/10.1016/j.foodres.2009.03.019.

(61) Zeng, Q. H.; Yu, A. B.; Lu, G. Q. (Max); Paul, D. R. Clay-Based Polymer Nanocomposites: Research and Commercial Development. *Journal of Nanoscience and Nanotechnology* **2005**, *5* (10), 1574–1592. https://doi.org/10.1166/jnn.2005.411.

(62) Liu, P. Polymer Modified Clay Minerals: A Review. *Applied Clay Science* **2007**, *38* (1), 64–76. https://doi.org/10.1016/j.clay.2007.01.004.

(63) Vasudeo Rane, A.; Kanny, K.; Abitha, V. K.; Patil, S. S.; Thomas, S. Chapter 4 - Clay–Polymer Composites: Design of Clay Polymer Nanocomposite by Mixing. In *Clay-Polymer Nanocomposites*; Jlassi, K., Chehimi, M. M., Thomas, S., Eds.; Elsevier, 2017; pp 113–144. https://doi.org/10.1016/B978-0-323-46153-5.00004-5.

(64) Rane, A. V.; Kanny, K.; Abitha, V. K.; Thomas, S. Chapter 5 - Methods for Synthesis of Nanoparticles and Fabrication of Nanocomposites. In *Synthesis of Inorganic Nanomaterials*; Mohan Bhagyaraj, S., Oluwafemi, O. S., Kalarikkal, N., Thomas, S., Eds.; Micro and Nano Technologies; Woodhead Publishing, 2018; pp 121–139. https://doi.org/10.1016/B978-0-08-101975-7.00005-1.

(65) Tang, X. Z.; Kumar, P.; Alavi, S.; Sandeep, K. P. Recent Advances in Biopolymers and Biopolymer-Based Nanocomposites for Food Packaging Materials. *Critical Reviews in Food Science and Nutrition* **2012**, *52* (5), 426–442. https://doi.org/10.1080/10408398.2010.500508.

(66) Vaia, R. A.; Ishii, H.; Giannelis, E. P. Synthesis and Properties of Two-Dimensional Nanostructures by Direct Intercalation of Polymer Melts in Layered Silicates. *Chem. Mater.* **1993**, *5* (12), 1694–1696. https://doi.org/10.1021/cm00036a004.

(67) Song, Y.; Lugo, E. L.; Powell, S.; Tzeng, P.; Wilhite, B. A.; Grunlan, J. C. Highly Selective Multilayer Polymer Thin Films for CO_2 /N_2 Separation. *J. Polym. Sci. Part B: Polym. Phys.* **2017**, *55* (23), 1730–1737. https://doi.org/10.1002/polb.24421.

(68) Qin, S.; Song, Y.; Floto, M. E.; Grunlan, J. C. Combined High Stretchability and Gas Barrier in Hydrogen-Bonded Multilayer Nanobrick Wall Thin Films. *ACS Appl. Mater. Interfaces* **2017**, *9* (9), 7903–7907. https://doi.org/10.1021/acsami.7b00844.

(69) Kotov, N. A.; Magonov, S.; Tropsha, E. Layer-by-Layer Self-Assembly of Alumosilicate−Polyelectrolyte Composites: Mechanism of Deposition, Crack Resistance, and Perspectives for Novel Membrane Materials. *Chem. Mater.* **1998**, *10* (3), 886–895. https://doi.org/10.1021/cm970649b.

(70) Zhao, L.; Yuan, B.; Geng, Y.; Yu, C.; Kim, N. H.; Lee, J. H.; Li, P. Fabrication of Ultrahigh Hydrogen Barrier Polyethyleneimine/Graphene Oxide Films by LBL Assembly Fine-Tuned with Electric Field Application. *Composites Part A: Applied Science and Manufacturing* **2015**, *78*, 60–69. https://doi.org/10.1016/j.compositesa.2015.07.020.

(71) Cho, C.; Xiang, F.; Wallace, K. L.; Grunlan, J. C. Combined Ionic and Hydrogen Bonding in Polymer Multilayer Thin Film for High Gas Barrier and Stretchiness. *Macromolecules* **2015**, *48* (16), 5723–5729. https://doi.org/10.1021/acs.macromol.5b01279.

(72) Yan, N.; Capezzuto, F.; Buonocore, G. G.; Lavorgna, M.; Xia, H.; Ambrosio, L. Gas-Barrier Hybrid Coatings by the Assembly of Novel Poly(Vinyl Alcohol) and Reduced Graphene Oxide Layers through Cross-Linking with Zirconium Adducts. *ACS Appl. Mater. Interfaces* **2015**, *7* (40), 22678–22685. https://doi.org/10.1021/acsami.5b07529.

(73) Hagen, D. A.; Saucier, L.; Grunlan, J. C. Controlling Effective Aspect Ratio and Packing of Clay with PH for Improved Gas Barrier in Nanobrick Wall Thin Films. *ACS Appl. Mater. Interfaces* **2014**, *6* (24), 22914–22919. https://doi.org/10.1021/am507603z.

(74) Priolo, M. A.; Gamboa, D.; Holder, K. M.; Grunlan, J. C. Super Gas Barrier of Transparent Polymer−Clay Multilayer Ultrathin Films. *Nano Lett.* **2010**, *10* (12), 4970–4974. https://doi.org/10.1021/nl103047k.

(75) Song, Y.; Hagen, D. A.; Qin, S.; Holder, K. M.; Falke, K.; Grunlan, J. C. Edge Charge Neutralization of Clay for Improved Oxygen Gas Barrier in Multilayer Nanobrick Wall Thin Films. *ACS Appl. Mater. Interfaces* **2016**, *8* (50), 34784–34790. https://doi.org/10.1021/acsami.6b12937.

(76) Yano, K.; Usuki, A.; Okada, A. Synthesis and Properties of Polyimide-Clay Hybrid Films. *Journal of Polymer Science Part A: Polymer Chemistry* **1997**, *35* (11), 2289–2294. https://doi.org/10.1002/(SICI)1099-0518(199708)35:11<2289::AID-POLA20>3.0.CO;2-9.

(77) Xu, R.; Manias, E.; Snyder, A. J.; Runt, J. Low Permeability Biomedical Polyurethane Nanocomposites. *Journal of Biomedical Materials Research Part A* **2003**, *64A* (1), 114–119. https://doi.org/10.1002/jbm.a.10377.

(78) Wang, Q.; Schlenoff, J. B. The Polyelectrolyte Complex/Coacervate Continuum. *Macromolecules* **2014**, *47* (9), 3108–3116. https://doi.org/10.1021/ma500500q.

(79) Fuoss, R. M.; Sadek, H. Mutual Interaction of Polyelectrolytes. *Science* **1949**, *110* (2865), 552–554. https://doi.org/10.1126/science.110.2865.552.

(80) Sun, J.; Perry, S. L.; Schiffman, J. D. Electrospinning Nanofibers from Chitosan/Hyaluronic Acid Complex Coacervates. *Biomacromolecules* **2019**, *20* (11), 4191–4198. https://doi.org/10.1021/acs.biomac.9b01072.

(81) Fu, J.; Schlenoff, J. B. Driving Forces for Oppositely Charged Polyion Association in Aqueous Solutions: Enthalpic, Entropic, but Not Electrostatic. *Journal of the American Chemical Society* **2016**, *138* (3), 980–990. https://doi.org/10.1021/jacs.5b11878.

(82) Michaels, A. S. POLYELECTROLYTE COMPLEXES. *Ind. Eng. Chem.* **1965**, *57* (10), 32–40. https://doi.org/10.1021/ie50670a007.

(83) de Jong, H. G. B.; Kruyt, H. R. Koazervation. *Kolloid-Zeitschrift* **1930**, *50* (1), 39–48. https://doi.org/10.1007/BF01422833.

(84) Zhang, Y.; Yildirim, E.; Antila, H. S.; Valenzuela, L. D.; Sammalkorpi, M.; Lutkenhaus, J. L. The Influence of Ionic Strength and Mixing Ratio on the Colloidal Stability of PDAC/PSS Polyelectrolyte Complexes. *Soft Matter* **2015**, *11* (37), 7392–7401. https://doi.org/10.1039/C5SM01184A.

(85) Perry, S. L.; Li, Y.; Priftis, D.; Leon, L.; Tirrell, M. The Effect of Salt on the Complex Coacervation of Vinyl Polyelectrolytes. *Polymers* **2014**, *6* (6), 1756–1772. https://doi.org/10.3390/polym6061756.

(86) Kelly, K. D.; Schlenoff, J. B. Spin-Coated Polyelectrolyte Coacervate Films. *ACS Appl. Mater. Interfaces* **2015**, *7* (25), 13980–13986. https://doi.org/10.1021/acsami.5b02988.

(87) Priftis, D.; Megley, K.; Laugel, N.; Tirrell, M. Complex Coacervation of Poly(Ethylene-Imine)/Polypeptide Aqueous Solutions: Thermodynamic and Rheological Characterization. *Journal of Colloid and Interface Science* **2013**, *398*, 39–50. https://doi.org/10.1016/j.jcis.2013.01.055.

(88) Chollakup, R.; Smitthipong, W.; Eisenbach, C. D.; Tirrell, M. Phase Behavior and Coacervation of Aqueous Poly(Acrylic Acid)−Poly(Allylamine) Solutions. *Macromolecules* **2010**, *43* (5), 2518–2528. https://doi.org/10.1021/ma902144k.

(89) Fu, J.; Fares, H. M.; Schlenoff, J. B. Ion-Pairing Strength in Polyelectrolyte Complexes. *Macromolecules* **2017**, *50* (3), 1066–1074. https://doi.org/10.1021/acs.macromol.6b02445.

(90) Iler, R. K. Multilayers of Colloidal Particles. *Journal of Colloid and Interface Science* **1966**, *21* (6), 569–594. https://doi.org/10.1016/0095-8522(66)90018-3.

(91) Decher, G.; Hong, J. D.; Schmitt, J. Buildup of Ultrathin Multilayer Films by a Self-Assembly Process: III. Consecutively Alternating Adsorption of Anionic and Cationic Polyelectrolytes on Charged Surfaces. *Thin Solid Films* **1992**, *210–211*, 831–835. https://doi.org/10.1016/0040-6090(92)90417-A.

(92) Decher, G.; Hong, J. D. Buildup of Ultrathin Multilayer Films by a Self-Assembly Process: II. Consecutive Adsorption of Anionic and Cationic Bipolar Amphiphiles and Polyelectrolytes on Charged Surfaces. *Berichte der Bunsengesellschaft für physikalische Chemie* **1991**, *95* (11), 1430–1434. https://doi.org/10.1002/bbpc.19910951122.

(93) Decher, G.; Schlenoff, J. B. *Multilayer Thin Films: Sequential Assembly of Nanocomposite Materials, Second Edition*; John Wiley & Sons, Ltd, 2012.

(94) Richardson, J. J.; Björnmalm, M.; Caruso, F. Technology-Driven Layer-by-Layer Assembly of Nanofilms. *Science* **2015**, *348* (6233). https://doi.org/10.1126/science.aaa2491.

(95) Jaber, J. A.; Schlenoff, J. B. Recent Developments in the Properties and Applications of Polyelectrolyte Multilayers. *Current Opinion in Colloid & Interface Science* **2006**, *11* (6), 324–329. https://doi.org/10.1016/j.cocis.2006.09.008.

(96) Zhang, Y.; Batys, P.; O'Neal, J. T.; Li, F.; Sammalkorpi, M.; Lutkenhaus, J. L. Molecular Origin of the Glass Transition in Polyelectrolyte Assemblies. *ACS Central Science* **2018**, *4* (5), 638–644. https://doi.org/10.1021/acscentsci.8b00137.

(97) Decher, G. Fuzzy Nanoassemblies: Toward Layered Polymeric Multicomposites. *Science* **1997**, *277* (5330), 1232–1237. https://doi.org/10.1126/science.277.5330.1232.

(98) Trigueiro, J. P. C.; Silva, G. G.; Pereira, F. V.; Lavall, R. L. Layer-by-Layer Assembled Films of Multi-Walled Carbon Nanotubes with Chitosan and Cellulose Nanocrystals. *Journal of Colloid and Interface Science* **2014**, *432*, 214–220. https://doi.org/10.1016/j.jcis.2014.07.001.

(99) Dierendonck, M.; Koker, S. D.; Rycke, R. D.; Geest, B. G. D. Just Spray It – LbL Assembly Enters a New Age. *Soft Matter* **2014**, *10* (6), 804–807. https://doi.org/10.1039/C3SM52202D.

(100) Hu, H.; Pauly, M.; Felix, O.; Decher, G. Spray-Assisted Alignment of Layer-by-Layer Assembled Silver Nanowires: A General Approach for the Preparation of Highly Anisotropic Nano-Composite Films. *Nanoscale* **2017**, *9* (3), 1307–1314. https://doi.org/10.1039/C6NR08045F.

(101) Xiang, F.; Givens, T. M.; Grunlan, J. C. Fast Spray Deposition of Super Gas Barrier Polyelectrolyte Multilayer Thin Films. *Ind. Eng. Chem. Res.* **2015**, *54* (19), 5254–5260. https://doi.org/10.1021/acs.iecr.5b01367.

(102) Lee, S.-S.; Hong, J.-D.; Kim, C. H.; Kim, K.; Koo, J. P.; Lee, K.-B. Layer-by-Layer Deposited Multilayer Assemblies of Ionene-Type Polyelectrolytes Based on the Spin-Coating Method. *Macromolecules* **2001**, *34* (16), 5358–5360. https://doi.org/10.1021/ma0022304.

(103) Karahan, H. E.; Eyüboğlu, L.; Kıyılar, D.; Demirel, A. L. PH-Stability and PH-Annealing of H-Bonded Multilayer Films Prepared by Layer-by-Layer Spin-Assembly. *European Polymer Journal* **2014**, *56*, 159–167. https://doi.org/10.1016/j.eurpolymj.2014.04.015.

(104) Cui, L.-Y.; Cheng, S.-C.; Liang, L.-X.; Zhang, J.-C.; Li, S.-Q.; Wang, Z.-L.; Zeng, R.-C. In Vitro Corrosion Resistance of Layer-by-Layer Assembled Polyacrylic Acid Multilayers Induced Ca–P Coating on Magnesium Alloy AZ31. *Bioact Mater* **2020**, *5* (1), 153–163. https://doi.org/10.1016/j.bioactmat.2020.02.001.

(105) Kharlampieva, E.; Sukhishvili, S. A. Hydrogen-Bonded Layer-by-Layer Polymer Films. *Journal of Macromolecular Science, Part C* **2006**, *46* (4), 377–395. https://doi.org/10.1080/15583720600945386.

(106) *A new approach for the fabrication of an alternating multilayer film of poly(4-vinylpyridine) and poly(acrylic acid) based on hydrogen bonding - Wang - 1997 - Macromolecular Rapid Communications - Wiley Online Library*. https://onlinelibrary.wiley.com/doi/10.1002/marc.1997.030180609 (accessed 2022-05-05).

(107) Xiang, F.; Ward, S. M.; Givens, T. M.; Grunlan, J. C. Structural Tailoring of Hydrogen-Bonded Poly(Acrylic Acid)/Poly(Ethylene Oxide) Multilayer Thin Films for Reduced Gas Permeability. *Soft Matter* **2015**, *11* (5), 1001–1007. https://doi.org/10.1039/C4SM02363C.

(108) Nestler, P.; Block, S.; Helm, C. A. Temperature-Induced Transition from Odd–Even to Even–Odd Effect in Polyelectrolyte Multilayers Due to Interpolyelectrolyte Interactions. *J. Phys. Chem. B* **2012**, *116* (4), 1234–1243. https://doi.org/10.1021/jp208837m.

(109) Tan, H. L.; McMurdo, M. J.; Pan, G.; Van Patten, P. G. Temperature Dependence of Polyelectrolyte Multilayer Assembly. *Langmuir* **2003**, *19* (22), 9311–9314. https://doi.org/10.1021/la035094f.

(110) Chang, L.; Kong, X.; Wang, F.; Wang, L.; Shen, J. Layer-by-Layer Assembly of Poly (N-Acryloyl-N'-Propylpiperazine) and Poly (Acrylic Acid): Effect of PH and

Temperature. *Thin Solid Films* **2008**, *516* (8), 2125–2129. https://doi.org/10.1016/j.tsf.2007.07.188.

(111) Shiratori, S. S.; Rubner, M. F. PH-Dependent Thickness Behavior of Sequentially Adsorbed Layers of Weak Polyelectrolytes. *Macromolecules* **2000**, *33* (11), 4213–4219. https://doi.org/10.1021/ma991645q.

(112) Izumrudov, V.; Sukhishvili, S. A. Ionization-Controlled Stability of Polyelectrolyte Multilayers in Salt Solutions. *Langmuir* **2003**, *19* (13), 5188–5191. https://doi.org/10.1021/la034360m.

(113) Dubas, S. T.; Schlenoff, J. B. Swelling and Smoothing of Polyelectrolyte Multilayers by Salt. *Langmuir* **2001**, *17* (25), 7725–7727. https://doi.org/10.1021/la0112099.

(114) Gong, X.; Gao, C. Influence of Salt on Assembly and Compression of PDADMAC/PSSMA Polyelectrolyte Multilayers. *Phys. Chem. Chem. Phys.* **2009**, *11* (48), 11577–11586. https://doi.org/10.1039/B915335G.

(115) Apaydin, K.; Laachachi, A.; Ball, V.; Jimenez, M.; Bourbigot, S.; Toniazzo, V.; Ruch, D. Polyallylamine–Montmorillonite as Super Flame Retardant Coating Assemblies by Layer-by Layer Deposition on Polyamide. *Polymer Degradation and Stability* **2013**, *98* (2), 627–634. https://doi.org/10.1016/j.polymdegradstab.2012.11.006.

(116) Guin, T.; Krecker, M.; Hagen, D. A.; Grunlan, J. C. Thick Growing Multilayer Nanobrick Wall Thin Films: Super Gas Barrier with Very Few Layers. *Langmuir* **2014**, *30* (24), 7057–7060. https://doi.org/10.1021/la501946f.

(117) Humood, M.; Chowdhury, S.; Song, Y.; Tzeng, P.; Grunlan, J. C.; Polycarpou, A. A. Nanomechanical Behavior of High Gas Barrier Multilayer Thin Films. *ACS Appl. Mater. Interfaces* **2016**, *8* (17), 11128–11138. https://doi.org/10.1021/acsami.5b11478.

(118) Yang, Y.-H.; Haile, M.; Park, Y. T.; Malek, F. A.; Grunlan, J. C. Super Gas Barrier of All-Polymer Multilayer Thin Films. *Macromolecules* **2011**, *44* (6), 1450–1459. https://doi.org/10.1021/ma1026127.

(119) Hagen, D. A.; Box, C.; Greenlee, S.; Xiang, F.; Regev, O.; Grunlan, J. C. High Gas Barrier Imparted by Similarly Charged Multilayers in Nanobrick Wall Thin Films. *RSC Adv.* **2014**, *4* (35), 18354–18359. https://doi.org/10.1039/C4RA01621A.

(120) Kim, Y. S.; Davis, R. Multi-Walled Carbon Nanotube Layer-by-Layer Coatings with a Trilayer Structure to Reduce Foam Flammability. *Thin Solid Films* **2014**, *550*, 184–189. https://doi.org/10.1016/j.tsf.2013.10.167.

(121) Tzeng, P.; Maupin, C. R.; Grunlan, J. C. Influence of Polymer Interdiffusion and Clay Concentration on Gas Barrier of Polyelectrolyte/Clay Nanobrick Wall Quadlayer Assemblies. *Journal of Membrane Science* **2014**, *452*, 46–53. https://doi.org/10.1016/j.memsci.2013.10.039.

(122) Tzeng, P.; Stevens, B.; Devlaming, I.; Grunlan, J. C. Polymer–Graphene Oxide Quadlayer Thin-Film Assemblies with Improved Gas Barrier. *Langmuir* **2015**, *31* (21), 5919–5927. https://doi.org/10.1021/acs.langmuir.5b00717.

(123) Podsiadlo, P.; Michel, M.; Lee, J.; Verploegen, E.; Wong Shi Kam, N.; Ball, V.; Lee, J.; Qi, Y.; Hart, A. J.; Hammond, P. T.; Kotov, N. A. Exponential Growth of LBL Films with Incorporated Inorganic Sheets. *Nano Lett.* **2008**, *8* (6), 1762–1770. https://doi.org/10.1021/nl8011648.

(124) Holder, K. M.; Smith, R. J.; Grunlan, J. C. A Review of Flame Retardant Nanocoatings Prepared Using Layer-by-Layer Assembly of Polyelectrolytes. *J Mater Sci* **2017**, *52* (22), 12923–12959. https://doi.org/10.1007/s10853-017-1390-1.

(125) Lazar, S. T.; Kolibaba, T. J.; Grunlan, J. C. Flame-Retardant Surface Treatments. *Nat Rev Mater* **2020**, *5* (4), 259–275. https://doi.org/10.1038/s41578-019-0164-6.

(126) Shimomura, H.; Gemici, Z.; Cohen, R. E.; Rubner, M. F. Layer-by-Layer-Assembled High-Performance Broadband Antireflection Coatings. *ACS Appl. Mater. Interfaces* **2010**, *2* (3), 813–820. https://doi.org/10.1021/am900883f.

(127) Eshaghi, A.; Mojab, M. Fabrication of Antireflective Antifogging Nano-Porous Silica Thin Film on Glass Substrate by Layer-by-Layer Assembly Method. *Journal of Non-Crystalline Solids* **2014**, *405*, 148–152. https://doi.org/10.1016/j.jnoncrysol.2014.09.017.

(128) Long, C. T.; Chen, L.; Iverson, E. T.; Castaneda, H.; Grunlan, J. C. Cross-Linking and Silanization of Clay-Based Multilayer Films for Improved Corrosion Protection of Steel. *J Mater Sci* **2022**, *57* (4), 2988–2998. https://doi.org/10.1007/s10853-021-06706-3.

(129) Qin, S.; Cubides, Y.; Lazar, S.; Ly, R.; Song, Y.; Gerringer, J.; Castaneda, H.; Grunlan, J. C. Ultrathin Transparent Nanobrick Wall Anticorrosion Coatings. *ACS Appl. Nano Mater.* **2018**, *1* (10), 5516–5523. https://doi.org/10.1021/acsanm.8b01032.

(130) Iverson, E. T.; Chiang, H.-C.; Kolibaba, T. J.; Schmieg, K.; Grunlan, J. C. Extraordinarily High Dielectric Breakdown Strength of Multilayer Polyelectrolyte Thin Films. *Macromolecules* **2022**, *55* (8), 3151–3158. https://doi.org/10.1021/acs.macromol.2c00259.

(131) Porcel, C. H.; Izquierdo, A.; Ball, V.; Decher, G.; Voegel, J.-C.; Schaaf, P. Ultrathin Coatings and (Poly(Glutamic Acid)/Polyallylamine) Films Deposited by Continuous and Simultaneous Spraying. *Langmuir* **2005**, *21* (2), 800–802. https://doi.org/10.1021/la047570n.

(132) Sato, H.; Takimoto, K.; Kato, M.; Nagaoka, S.; Tamura, K.; Yamagishi, A. Real-Time Monitoring of Low Pressure Oxygen Molecules over Wide Temperature Range: Feasibility of Ultrathin Hybrid Films of Iridium(III) Complexes and Clay Nanosheets. *BCSJ* **2019**, *93* (2), 194–199. https://doi.org/10.1246/bcsj.20190277.

(133) Lagaron, J. M.; Catalá, R.; Gavara, R. Structural Characteristics Defining High Barrier Properties in Polymeric Materials. *Materials Science and Technology* **2004**, *20* (1), 1–7. https://doi.org/10.1179/026708304225010442.

(134) Walther, A.; Bjurhager, I.; Malho, J.-M.; Pere, J.; Ruokolainen, J.; Berglund, L. A.; Ikkala, O. Large-Area, Lightweight and Thick Biomimetic Composites with Superior Material Properties via Fast, Economic, and Green Pathways. *Nano Lett.* **2010**, *10* (8), 2742–2748. https://doi.org/10.1021/nl1003224.

(135) Lazar, S.; Garcia-Valdez, O.; Kennedy, E.; Champagne, P.; Cunningham, M.; Grunlan, J. Crosslinkable-Chitosan-Enabled Moisture-Resistant Multilayer Gas Barrier Thin Film. *Macromol. Rapid Commun.* **2019**, *40* (6), 1800853. https://doi.org/10.1002/marc.201800853.

(136) Richert, L.; Boulmedais, F.; Lavalle, P.; Mutterer, J.; Ferreux, E.; Decher, G.; Schaaf, P.; Voegel, J.-C.; Picart, C. Improvement of Stability and Cell Adhesion Properties of Polyelectrolyte Multilayer Films by Chemical Cross-Linking. *Biomacromolecules* **2004**, *5* (2), 284–294. https://doi.org/10.1021/bm0342281.

(137) Yang, Y.-H.; Bolling, L.; Haile, M.; Grunlan, J. C. Improving Oxygen Barrier and Reducing Moisture Sensitivity of Weak Polyelectrolyte Multilayer Thin Films with Crosslinking. *RSC Adv.* **2012**, *2* (32), 12355. https://doi.org/10.1039/c2ra21845c.

(138) Tong, W.; Gao, C.; Möhwald, H. Manipulating the Properties of Polyelectrolyte Microcapsules by Glutaraldehyde Cross-Linking. *Chem. Mater.* **2005**, *17* (18), 4610–4616. https://doi.org/10.1021/cm0507516.

(139) Li, J.; van Ewijk, G.; van Dijken, D. J.; van der Gucht, J.; de Vos, W. M. Single-Step Application of Polyelectrolyte Complex Films as Oxygen Barrier Coatings.

ACS Appl. Mater. Interfaces **2021**, *13* (18), 21844–21853. https://doi.org/10.1021/acsami.1c05031.

(140) Demadis, K. D.; Paspalaki, M.; Theodorou, J. Controlled Release of Bis(Phosphonate) Pharmaceuticals from Cationic Biodegradable Polymeric Matrices. *Ind. Eng. Chem. Res.* **2011**, *50* (9), 5873–5876. https://doi.org/10.1021/ie102546g.

(141) Swift, T.; Swanson, L.; Geoghegan, M.; Rimmer, S. The PH-Responsive Behaviour of Poly(Acrylic Acid) in Aqueous Solution Is Dependent on Molar Mass. *Soft Matter* **2016**, *12* (9), 2542–2549. https://doi.org/10.1039/C5SM02693H.

(142) Sun, Y.; Peng, C.; Wang, X.; Wang, R.; Chen, Y.; Zhang, D. Phase Behavior of Polyelectrolyte Complexes and Rheological Behavior of Alumina Suspensions for Direct Ink Writing. *Journal of the American Ceramic Society* **2016**, *99* (6), 1902–1910. https://doi.org/10.1111/jace.14155.

(143) Kong, H. J.; Mooney, D. J. The Effects of Poly(Ethyleneimine) (PEI) Molecular Weight on Reinforcement of Alginate Hydrogels. *Cell Transplant* **2003**, *12* (7), 779–785. https://doi.org/10.3727/000000003108747253.

(144) Choi, J.; Rubner, M. F. Influence of the Degree of Ionization on Weak Polyelectrolyte Multilayer Assembly. *Macromolecules* **2005**, *38* (1), 116–124. https://doi.org/10.1021/ma048596o.

(145) Aulin, C.; Karabulut, E.; Tran, A.; Wågberg, L.; Lindström, T. Transparent Nanocellulosic Multilayer Thin Films on Polylactic Acid with Tunable Gas Barrier Properties. *ACS Appl. Mater. Interfaces* **2013**, *5* (15), 7352–7359. https://doi.org/10.1021/am401700n.

(146) Schmidt-Traub, G.; Obersteiner, M.; Mosnier, A. Fix the Broken Food System in Three Steps. *Nature* **2019**, *569* (7755), 181–183. https://doi.org/10.1038/d41586-019-01420-2.

(147) FAO. Global Food Losses and Food Waste, 2011.

(148) Mehyar, G. F.; Han, J. H. Active Packaging for Fresh-Cut Fruits and Vegetables. In *Modified Atmosphere Packaging for Fresh-Cut Fruits and Vegetables*; John Wiley & Sons, Ltd, 2011; pp 267–283. https://doi.org/10.1002/9780470959145.ch14.

(149) Koushesh Saba, M.; Sogvar, O. B. Combination of Carboxymethyl Cellulose-Based Coatings with Calcium and Ascorbic Acid Impacts in Browning and

Quality of Fresh-Cut Apples. *LWT - Food Science and Technology* **2016**, *66*, 165–171. https://doi.org/10.1016/j.lwt.2015.10.022.

(150) Perez-Gago, M. B.; Serra, M.; Alonso, M.; Mateos, M.; Río, M. A. D. Effect of Solid Content and Lipid Content of Whey Protein Isolate-Beeswax Edible Coatings on Color Change of Fresh-Cut Apples. *Journal of Food Science* **2003**, *68* (7), 2186–2191. https://doi.org/10.1111/j.1365-2621.2003.tb05744.x.

(151) Guidotti, G.; Soccio, M.; García-Gutiérrez, M. C.; Ezquerra, T.; Siracusa, V.; Gutiérrez-Fernández, E.; Munari, A.; Lotti, N. Fully Biobased Superpolymers of 2,5-Furandicarboxylic Acid with Different Functional Properties: From Rigid to Flexible, High Performant Packaging Materials. *ACS Sustainable Chemistry & Engineering* **2020**. https://doi.org/10.1021/acssuschemeng.0c02840.

(152) Goulas, A. E. Overall Migration from Commercial Coextruded Food Packaging Multilayer Films and Plastics Containers into Official EU Food Simulants. *European Food Research and Technology* **2001**, *212* (5), 597–602. https://doi.org/10.1007/s002170000294.

(153) Marsh, K.; Bugusu, B. Food Packaging - Roles, Materials, and Environmental Issues: Scientific Status Summary. *Journal of Food Science* **2007**, *72* (3). https://doi.org/10.1111/j.1750-3841.2007.00301.x.

(154) Ruggeri, E.; Kim, D.; Cao, Y.; Farè, S.; De Nardo, L.; Marelli, B. A Multilayered Edible Coating to Extend Produce Shelf Life. *ACS Sustainable Chem. Eng.* **2020**, *8* (38), 14312–14321. https://doi.org/10.1021/acssuschemeng.0c03365.

(155) Jung, S.; Cui, Y.; Barnes, M.; Satam, C.; Zhang, S.; Chowdhury, R. A.; Adumbumkulath, A.; Sahin, O.; Miller, C.; Sajadi, S. M.; Sassi, L. M.; Ji, Y.; Bennett, M. R.; Yu, M.; Friguglietti, J.; Merchant, F. A.; Verduzco, R.; Roy, S.; Vajtai, R.; Meredith, J. C.; Youngblood, J. P.; Koratkar, N.; Rahman, M. M.; Ajayan, P. M. Multifunctional Bio-Nanocomposite Coatings for Perishable Fruits. *Adv. Mater.* **2020**, 1908291. https://doi.org/10.1002/adma.201908291.

(156) Sriamornsak, P.; Kennedy, R. A. A Novel Gel Formation Method, Microstructure and Mechanical Properties of Calcium Polysaccharide Gel Films. *International Journal of Pharmaceutics* **2006**, *323* (1), 72–80. https://doi.org/10.1016/j.ijpharm.2006.05.045.

(157) Benbettaïeb, N.; Kurek, M.; Bornaz, S.; Debeaufort, F. Barrier, Structural and Mechanical Properties of Bovine Gelatin–Chitosan Blend Films Related to Biopolymer Interactions. *Journal of the Science of Food and Agriculture* **2014**, *94* (12), 2409–2419. https://doi.org/10.1002/jsfa.6570.

(158) Laufer, G.; Kirkland, C.; Cain, A. A.; Grunlan, J. C. Oxygen Barrier of Multilayer Thin Films Comprised of Polysaccharides and Clay. *Carbohydrate Polymers* **2013**, *95* (1), 299–302. https://doi.org/10.1016/j.carbpol.2013.02.048.

(159) Zargar, V.; Asghari, M.; Dashti, A. A Review on Chitin and Chitosan Polymers: Structure, Chemistry, Solubility, Derivatives, and Applications. *ChemBioEng Reviews* **2015**, *2* (3), 204–226. https://doi.org/10.1002/cben.201400025.

(160) Hamman, J. H. Chitosan Based Polyelectrolyte Complexes as Potential Carrier Materials in Drug Delivery Systems. *Mar Drugs* **2010**, *8* (4), 1305–1322. https://doi.org/10.3390/md8041305.

(161) Andrady, A. L.; Xu, P. Elastic Behavior of Chitosan Films. *Journal of Polymer Science Part B: Polymer Physics* **1997**, *35* (3), 517–521. https://doi.org/10.1002/(SICI)1099-0488(199702)35:3<517::AID-POLB10>3.0.CO;2-K.

(162) Chang, L.-W.; Lytle, T. K.; Radhakrishna, M.; Madinya, J. J.; Vélez, J.; Sing, C. E.; Perry, S. L. Sequence and Entropy-Based Control of Complex Coacervates. *Nature Communications* **2017**, *8* (1), 1273. https://doi.org/10.1038/s41467-017-01249-1.

(163) Mohammed, M. A.; Syeda, J. T. M.; Wasan, K. M.; Wasan, E. K. An Overview of Chitosan Nanoparticles and Its Application in Non-Parenteral Drug Delivery. *Pharmaceutics* **2017**, *9* (4). https://doi.org/10.3390/pharmaceutics9040053.

(164) Celus, M.; Kyomugasho, C.; Loey, A. M. V.; Grauwet, T.; Hendrickx, M. E. Influence of Pectin Structural Properties on Interactions with Divalent Cations and Its Associated Functionalities. *Comprehensive Reviews in Food Science and Food Safety* **2018**, *17* (6), 1576–1594. https://doi.org/10.1111/1541-4337.12394.

(165) Song, Y.; Meyers, K. P.; Gerringer, J.; Ramakrishnan, R. K.; Humood, M.; Qin, S.; Polycarpou, A. A.; Nazarenko, S.; Grunlan, J. C. Fast Self-Healing of Polyelectrolyte Multilayer Nanocoating and Restoration of Super Oxygen Barrier. *Macromol. Rapid Commun.* **2017**, *38* (10), 1700064. https://doi.org/10.1002/marc.201700064.

(166) *Nacre-mimetic composite with intrinsic self-healing and shape-programming capability | Nature Communications*. https://www.nature.com/articles/s41467-019-08643-x (accessed 2020-10-29).

(167) *Thermoreversible Networks by Diels–Alder Reaction of Cellulose Furoates With Bismaleimides - Ax - 2012 - Macromolecular Chemistry and Physics - Wiley Online Library*.

https://onlinelibrary.wiley.com/doi/abs/10.1002/macp.201100410 (accessed 2020-10-29).

(168) Froidevaux, V.; Borne, M.; Laborbe, E.; Auvergne, R.; Gandini, A.; Boutevin, B. Study of the Diels–Alder and Retro-Diels–Alder Reaction between Furan Derivatives and Maleimide for the Creation of New Materials. *RSC Adv.* **2015**, *5* (47), 37742–37754. https://doi.org/10.1039/C5RA01185J.

(169) Harris, J. J.; DeRose, P. M.; Bruening, M. L. Synthesis of Passivating, Nylon-Like Coatings through Cross-Linking of Ultrathin Polyelectrolyte Films. *J. Am. Chem. Soc.* **1999**, *121* (9), 1978–1979. https://doi.org/10.1021/ja9833467.

(170) Cardoso, D. R.; Libardi, S. H.; Skibsted, L. H. Riboflavin as a Photosensitizer. Effects on Human Health and Food Quality. *Food Funct.* **2012**, *3* (5), 487–502. https://doi.org/10.1039/C2FO10246C.

(171) *Effect of photochemical UV/riboflavin-mediated cross-links on different properties of fish gelatin films - Wang - 2017 - Journal of Food Process Engineering - Wiley Online Library*. https://onlinelibrary.wiley.com/doi/full/10.1111/jfpe.12536 (accessed 2020-10-29).

(172) Chan, E.; Snibson, G. R. Current Status of Corneal Collagen Cross-Linking for Keratoconus: A Review. *Clinical and Experimental Optometry* **2013**, *96* (2), 155–164. https://doi.org/10.1111/cxo.12020.

(173) Kato, Y.; Uchida, K.; Kawakishi, S. Aggregation of Collagen Exposed to Uva in the Presence of Riboflavin: A Plausible Role of Tyrosine Modification. *Photochemistry and Photobiology* **1994**, *59* (3), 343–349. https://doi.org/10.1111/j.1751-1097.1994.tb05045.x.